Aerosol optical, microphysical and radiative properties at regional background insular sites in the western Mediterranean

Michaël Sicard[1,2], Rubén Barragan[1,2], François Dulac[3], Lucas Alados-Arboledas[4,5], Marc Mallet[6]

[1]Remote Sensing Laboratory, Universitat Politècnica de Catalunya, Barcelona, Spain

[2]Ciències i Tecnologies de l'Espai - Centre de Recerca de l'Aeronàutica i de l'Espai / Institut d'Estudis Espacials de Catalunya (CTE-CRAE / IEEC), Universitat Politècnica de Catalunya, Barcelona, Spain

[3]Laboratoire des Sciences du Climat et de l'Environement, (IPSL/LSCE), CEA-CNRS-UVSQ, Université Paris-Saclay, Gif-sur-Yvette, France

[4]Dpt. Applied Physics, Faculty of Sciences, University of Granada, Granada, Spain

[5]Andalusian Institute for Earth System Research (IISTA-CEAMA), Granada, Spain

[6]Laboratoire d'Aérologie, Université de Toulouse / CNRS, Toulouse, France

Correspondence to: msicard@tsc.upc.edu

Abstract

In the framework of the ChArMEx (the Chemistry-Aerosol Mediterranean Experiment, http://charmex.lsce.ipsl.fr/) program, the seasonal variability of the aerosol optical, microphysical and radiative properties derived from AERONET (Aerosol Robotic Network; http://aeronet.gsfc.nasa.gov/) is examined in two regional background insular sites in the western Mediterranean Basin: Ersa (Corsica Island, France) and Palma de Mallorca (Mallorca Island, Spain). A third site, Alborán (Alborán Island, Spain), with only a few months of data is considered for examining possible Northeast–Southwest (NE–SW) gradients of the aforementioned aerosol properties. The AERONET dataset is exclusively composed of level 2.0 inversion products available during the five-year period 2011-2015. AERONET solar radiative fluxes are validated with ground- and satellite-based flux measurements. To the best

of our knowledge this is the first time that AERONET fluxes are validated at the top of the atmosphere. The main drivers of the observed annual cycles and NE–SW gradients are 1) mineral dust outbreaks in spring in the North and in summer in the South, and 2) European pollution episodes in autumn. A NE–SW gradient exists in the western Mediterranean Basin for the aerosol optical depth and especially its coarse mode fraction, which all together produces a similar gradient for the aerosol direct radiative forcing. The aerosol fine mode is rather homogeneously distributed. Absorption properties are quite variable because of the many and different sources of anthropogenic particles in and around the western Mediterranean Basin: North African and European urban areas, the Iberian and Italian Peninsulas, forest fires and ship emissions. As a result the aerosol direct forcing efficiency, more dependent to absorption than the absolute forcing, has no marked gradient.

Short summary

The seasonal variability of the aerosol optical, microphysical and radiative properties at two insular sites in the western Mediterranean Basin is presented based on AERONET Level 2.0 data. The AERONET-derived surface and top of atmosphere radiative fluxes are validated with ground-based and satellite data, respectively. The main drivers of the observed annual cycles and NE–SW gradients are 1) mineral dust outbreaks in spring in the North and in summer in the South, and 2) European pollution episodes in autumn. The lack of NE–SW gradients of some aerosol properties is attributed to: a homogeneous spatial distribution of the fine particle load and a large variability of the absorption properties.

1 Introduction

Climate change projections identify the Mediterranean region as a climatologically sensitive area especially vulnerable to global change (Giorgi, 2006; Giorgi and Lionello, 2008). General and regional climate models simulate significant changes in the water cycle of the Meditterranean region, a substantial precipitation decrease and a temperature increase before the end of the century (Sanchez-Gomez et al., 2009; Mariotti et al., 2015). Atmospheric aerosols are one of the factors that influence the Mediterranean climate through their impact on the radiation budget (Markowicz et al., 2002; Nabat et al., 2014; 2015). Specifically, atmospheric aerosols influence the Earth's energy budget both directly, because they absorb and scatter solar and terrestrial radiation, and indirectly, because they act as cloud condensation

nuclei modifying the structure and the properties of clouds (Twomey, 1974; Albrecht, 1989; Pincus and Baker, 1994). How those impacts distribute themselves in space and time over the greater Mediterranean Basin remains an open question (Mallet et al., 2016).

The columnar amount of atmospheric aerosol, which can be quantified by the aerosol optical depth (AOD), has a direct effect on the solar and infrared radiation reaching the Earth's surface. An increase or decrease in AOD can result in enhanced or reduced solar radiation at the surface, an effect that Norris and Wild (2007) called solar "brightening" and "dimming", respectively. For that reason the AOD is often used to quantify the aerosol impact on the surface solar radiation. Numerous studies documenting the spatial variability of the AOD over the Mediterranean Basin are based on long time series of satellite-based observations (Barnaba and Gobbi, 2004; Papadimas et al., 2008; Nabat et al., 2012; 2013, among others) and in a lesser extent on ground-based remote sensing observations (Mallet et al., 2013; Lyamani et al., 2015, among others). The temporal variability of the AOD over the whole Mediterranean Basin has been assessed for the first time by Papadimas et al. (2008) using the AOD retrieved at 550 nm and the fine mode fraction of total AOD products (both over land and ocean) of the Moderate Resolution Imaging Spectroradiometer (MODIS) instrument during the period 2000-2006.

Although the AOD is a key parameter to understand the variability of the aerosol impact on the Earth's energy budget, its analysis is not enough to assess this variability at the scale of the Mediterranean Basin because of the great complexity of the aerosol composition and distribution over the Basin. Bounded to the North by the European continent and to the South by the African continent, the Mediterranean atmosphere is largely affected by maritime particles, urban/industrial aerosols from European and North African urban areas, extreme biomass burning episodes and mineral dust from North African arid areas. Anthropogenic particles emitted from ship traffic are also present all-year round while biomass burning aerosols from forest fires from both European and African continents are limited to the summer season. A detailed list of long term analyses or case studies about one or several types of those aerosols can be found in Mallet et al. (2016). All those aerosol types have very different optical, microphysical and radiative properties. Consequently, in addition to the AOD, other parameters like the absorption properties, the size of the particles, their shape, etc. are needed to assess the variability of the aerosol impact on the Earth's energy budget at the scale of the Mediterranean Basin.

In this study we perform a seasonal analysis of the aerosol optical, microphysical and radiative columnar properties at two regional background insular sites at Ersa (Corsica, France) and Palma de Mallorca (Mallorca, Spain) with data from a recent period (2011-2015). The dataset

is exclusively composed of AERONET (Aerosol Robotic Network; http://aeronet.gsfc) level 2.0 inversion products. Insular sites were selected in order to determine the properties of aerosols representative of the whole basin minimizing local influences. The choice of the western Mediterranean Basin was motivated by the ChArMEx (the Chemistry-Aerosol Mediterranean Experiment, http://charmex.lsce.ipsl.fr/) program which is a collaborative research program federating international activities to investigate Mediterranean regional chemistry-climate interactions. One of the goals of ChArMEx is precisely to improve our knowledge of the potential impacts of aerosols over the Mediterranean Basin (Dulac et al., 2014; Mallet et al., 2016). In its implementation strategy ChArMEx proposes Enhanced Observation Periods (EOP) to study the daily to seasonal scale variability of several parameters measured at several sites and to monitor East–West and North–South gradients over a period of 2-3 years. The AERONET sun-photometer from Ersa was deployed in that framework. In order to examine possible North–South gradients over the whole western Mediterranean Basin, and not only in its northern part, we complement the dataset with five months of coincident measurements in 2011 in the remote island of Alborán (Spain) between Spain and Morocco.

The paper is organized as follows: Section 2 of the paper presents the three sites, the dataset and details all the AERONET products used in the paper and their associated accuracy. The methodology used to perform a tentative aerosol classification is presented in Section 3. Atmospheric dynamics of the region is addressed in Section 4 with a general regional description in Section 4.1 and peculiarities of the aerosol loading specific to each of the three sites in Section 4.2. Differences in aerosol optical properties between Ersa and Palma are discussed in Section 5: in terms of monthly variations of the total AOD, Ångström exponent and fine mode fraction of total AOD (Section 5.1), particle volume size distribution (Section 5.2) and seasonal variation of the aerosol absorption optical depth, absorption Ångström exponent and the refractive index (Section 5.3), and single scattering albedo and asymmetry factor (Section 5.4). In order to go one step further, we also analyze the AERONET products of aerosol radiative forcing (Section 6). We first validate the fluxes estimated by AERONET with ground- and satellite-based flux measurements (Section 6.1) and then present the monthly variations of the aerosol radiative forcing and of the aerosol radiative forcing efficiency at both sites (Section 6.2). In addition, a discussion is proposed in Section 7 on the possible North–South gradients of the aerosol properties based on five months of coincident measurements in 2011 at Ersa, Palma and Alborán. Finally, conclusions are proposed in Section 8.

2 Sites and instrumentation

2.1 Sites

The sites selected for this analysis had to fulfill the following criteria: to be located in the western Mediterranean Basin, to be insular sites in order to be representative of aerosol regional background conditions, to be approximately aligned on a North–South axis and to have a recent long-term database (≥ 2 years). At the same time we wanted to take advantage of the ChArMEx EOP (2–3 years) in the framework of which a supersite was installed at the northern tip of Corsica Island (France), at Ersa (Lambert et al., 2011; Dulac et al., 2014, Mallet et al., 2016). In that site, situated at 43.00ºN, 9.36ºE, 80 m asl (above sea level), an AERONET sun-photometer is operated since June 2008. According to the AERONET Data Display Interface and applying the above mentioned criteria the second site that was selected is Palma de Mallorca in the Balearic Islands (Spain) situated at 39.55ºN, 2.62ºE, 10 m asl, and operated since August 2011. Both sites are on the Northeast–Southwest (NE–SW) axis, a major route for dust transport in the western Mediterranean Basin (Moulin et al., 1998). In the last Section of the paper, a third site considered for examining possible NE–SW gradients is Alborán (Spain, 35.94ºN, 3.04ºW, 15 m asl) situated East of Gibraltar midway between the Spanish and the Moroccan coasts. There, an AERONET sun-photometer was operated for a rather short period of time, between June 2011 and January 2012, thanks to collaboration between the Atmospheric Physic Group of the University of Granada and the Royal Institute and Observatory of the Spanish Navy. Indeed all three sites, reported in Figure 1, fall onto a quasi-perfect NE–SW straight line and Palma, situated in the middle, is approximately equidistant to both Ersa (~670 km) and Alborán (~640 km).

2.2 AERONET sun-photometers and products

AERONET is a federated network of ground-based sun-photometers (Holben et al., 1998) which retrieves global aerosol columnar properties. Along with aerosol optical depths at several wavelengths λ (AOD_λ), AERONET products are the Ångström exponent (AE) between pairs of wavelengths, the precipitable water vapor and the total, fine and coarse mode AOD at 500 nm derived from the Spectral Deconvolution Algorithm (SDA) from which the fine/coarse mode fractions can be calculated (O'Neill et al., 2001; 2003). Further AERONET inversion data products include volume size distribution, the spectral complex refractive index (real and imaginary), the spectral aerosol absorption optical depth, the spectral single scattering albedo, the spectral asymmetry factor, the spectral phase function and the sphericity, i.e. the volume

fraction of spherical particles (Dubovik et al., 2000a; 2002a; 2006; Sinyuk et al., 2007). A series of assumptions are made to perform the inversion of those parameters. They can be found in the AERONET Version 2 Inversion Product Descriptions (AERONET, 2016). All the inversion products spectrally resolved are given at 440, 675, 870 and 1020 nm.

The data shown in this work are based on AERONET level 2.0, cloud-screened and quality-assured data (Smirnov et al., 2000) inverted with the AERONET Version 2.0 retrieval algorithm (Holben et al., 2006). In practice the main differences between Version 1.0 and Version 2.0 are the additional criteria applied in Version 2.0 on: the solar zenith angle (SZA; $50 < SZA < 80^{o}$ for all products) and the AOD at 440 nm ($AOD_{440} > 0.4$ for the aerosol absorption optical depth, the single scattering albedo and the real and the imaginary parts of the refractive index; $AOD_{440} > 0.2$ for the sphericity). The accuracy of AERONET Version 2.0, level 2.0 inversion products is evaluated and discussed in Dubovik et al. (2000b; 2002b) and the additional criteria for Version 2.0 retrieval in Holben et al. (2006). The accuracy of some products has been estimated with numerical sensitivity tests for different aerosol types, namely water-soluble, dust and biomass burning (Dubovik et al., 2000b).

- The estimated accuracy of AOD_{λ} is ±0.02 (Eck et al., 1999).
- The accuracy of the Ångström exponent is estimated to be ±0.25 for $AOD_{440} \geq 0.1$ and of the order of 50 % for $AOD_{440} < 0.1$ (Toledano et al., 2007).
- The accuracy of the volume size distribution is estimated to be: 15 % for water-soluble, 35 % for dust and 25 % for biomass burning in the intermediate particle size range ($0.1 \leq$ radius $r \leq 7$ μm); and 15-100 % for water-soluble, 35-100 % for dust and 25-100 % for biomass burning for the edges ($0.05 \leq r < 0.1$ μm and $7 < r \leq 15$ μm).
- The accuracy of the real (imaginary in %) part of the refractive index is estimated to be ±0.025 (50 %) for $AOD_{440} > 0.2$ for water-soluble and ±0.04 (50 and 30 %, respectively) for $AOD_{440} \geq 0.5$ for dust and biomass burning.
- The retrieved aerosol absorption optical depth at wavelength λ ($AAOD_{\lambda}$) has an accuracy of ±0.01 at $\lambda \geq 440$ nm.
- The accuracy of the single scattering albedo at wavelength λ (SSA_{λ}) is estimated to be ±0.03 for $AOD_{440} > 0.2$ for water-soluble and for $AOD_{440} \geq 0.5$ for dust and biomass burning.
- The uncertainty of the asymmetry factor at wavelength λ (g_{λ}) ranges between ±0.03 and ±0.08 for pollution and biomass burning aerosols and is ±0.04 for desert dust particles.

It is important to note that some products such as the AAOD, the real and the imaginary parts of the refractive index and the SSA are retrieved only if the criterion $AOD_{440} > 0.4$ is fulfilled. Such aerosol loads are generally associated to desert dust outbreaks or severe pollution episodes (Gkikas et al., 2012; 2016).

Other parameters of interest for this work delivered by the AERONET inversion algorithm are the instantaneous solar broadband (0.2 – 4 μm) downward and upward fluxes, as well as the aerosol radiative forcing and radiative forcing efficiency at the surface and at the top of the atmosphere. A brief description on how the fluxes are calculated is given in the AERONET Version 2 Inversion Product Descriptions (AERONET, 2016). The gaseous absorption is calculated by the GAME (Global Atmospheric Model) radiative transfer model (Dubuisson et al., 1996). We consider all instantaneous measurements available.

3 Methodology

The methodology used to classify the aerosols based on AERONET level 2.0 inversion products is the graphical method from Gobbi et al. (2007). The Ångström exponent, calculated between two wavelengths λ_1 and λ_2, $AE_{\lambda_1-\lambda_2}$, and defined as

$$AE_{\lambda_1-\lambda_2} = -\frac{\ln\left[\frac{AOD_{\lambda_1}}{AOD_{\lambda_2}}\right]}{\ln\left[\frac{\lambda_1}{\lambda_2}\right]}, \quad (1)$$

is commonly used as a good indicator of the dominant size of the atmospheric particles contributing to the total AOD: values of AE < 1 indicate size distributions dominated by coarse mode aerosols (radii > 0.5 μm) while values of AE > 1.5 indicate size distributions dominated by fine mode aerosols. When different aerosol types are present in the atmospheric column, AE does not provide information on the relative contribution of coarse and fine mode particles. For this reason, the Ångström exponent difference is introduced and the Gobbi et al. (2007) method consists in deriving the Ångström exponent ($AE_{440\text{-}870}$) and the Ångström exponent difference ($\delta AE = AE_{440\text{-}675} - AE_{675\text{-}870}$), defined as a measure of the Ångström exponent curvature, $dAE/d\lambda$, the fine mode aerosol radius and the contribution of the fine mode aerosol to the total AOD. Several authors have investigated how the spectral variation of AE can provide further information on the aerosol size distribution (Schuster et al., 2006, and references therein). In particular Kaufman (1993) pointed out that negative values of $AE_{440\text{-}613} - AE_{440\text{-}1003}$ indicated the dominance of fine mode particles, while positive differences indicated the

effect of two separate modes with a significant coarse mode contribution. The graphical method developed by Gobbi et al. (2007) uses these complementarities between AE and δAE. The method has been applied, among others, by (i) Gobbi et al. (2007) at sites characterized by high pollution, biomass burning and/or mineral dust concentrations; (ii) Basart et al. (2009) to quantify the contribution of mineral dust on a yearly basis at sites in and around the Sahara – Sahel region; and (iii) Perrone et al. (2014) to distinguish between mostly pollution and mineral dust in Lecce, Italy.

Instantaneous values of the Ångström exponent difference vs. the Ångström exponent (δAE, AE) are plotted on a classification framework with reference points determined for a variety of fine mode (r^f) and coarse mode (r^c) radii and of fine mode fractions of total AOD (η). To this end, Mie calculations were performed to calculate the aerosol spectral extinction coefficients for r^f values of 0.05, 0.1, 0.15, 0.2, 0.3 and 0.5 μm, for r^c values of 0.75, 1, 2, and 4 μm, and η fractions of 1, 10, 30, 50, 70, 90 and 99 %, assuming a bimodal, lognormal size distribution. Each (δAE, AE) grid point is obtained as the average of the four pairs obtained for the four r^c values. The grid used in this paper was taken from Gobbi et al. (2007) with a refractive index of 1.4-0.001*i*, typical of urban/industrial aerosols, in order to both provide a common reference and address the relative changes (fine mode growth/hydration or coarse particle growth/cloud contamination, see Gobbi et al. (2007) for definition) at each location. As suggested by Gobbi et al. (2007), the condition $AOD_{675} > 0.15$ has been applied on all the (δAE, AE) plots in order to guarantee errors less than 30 % on δAE. The values of δAE in Table 1 are also given with this criterion: $AOD_{675} > 0.15$. Note, however, that the AOD plotted in the (δAE, AE) plots of the paper is AOD_{440} (and not AOD_{675}) in order to be directly comparable with the AERONET criteria based on AOD_{440}.

The seasonal variations shown in the paper are made for the following four seasons: summer (JJA, June-July-August), autumn (SON, September-October-November), winter (DJF, December-January-February) and spring (MAM, March-April-May).

4 Atmospheric dynamics

4.1 Atmospheric dynamics of the western Mediterranean Basin

The Mediterranean region features an almost enclosed sea surrounded by very urbanized littorals and important mountain barriers. The gaps between the major mountainous regions act as channels for the air mass transport toward the Mediterranean Basin which constitutes a crossroads of air masses carrying aerosols from different natural and anthropogenic sources

(Lelieveld et al., 2002). In particular in the western Mediterranean Basin those channels are the Strait of Gibraltar and the Ebro Valley in Spain, the Rhône Valley in France and the Po valley in Italy. The atmospheric dynamics of the western Mediterranean Basin is mainly governed by the extended subtropical anticyclone of the Atlantic (Azores anticyclone) and can be roughly divided into cold and warm periods (Maheras et al. 1999; Kallos et al., 2007), respectively associated with low and high aerosol loads. A significant amount of literature exists about the relationship between the synoptic conditions in the Mediterranean Basin and the occurrence of aerosol episodes (e.g. Moulin et al., 1998; Gangoiti et al., 2001; Lelieveld et al., 2002; Kallos et al., 2007, and papers cited therein; Papadimas et al., 2008; Gkikas et al., 2012).

In winter and part of spring, the Azores anticyclone presents its lowest intensity and usually stays west of the western Mediterranean Basin (Millán et al., 1997). Weak gradient anticyclonic conditions are recurrent over the western Mediterranean Basin and favor the stagnation of pollutants near populated and industrialized areas around the Basin (Lyamani et al., 2012). The thermal inversions associated to such anticyclonic conditions and the local breezes that may be activated by solar radiation help the pollutants to disperse over the Basin. Winter is also the time when the Azores anticyclone leaves room to an anticyclone that may form over the Bay of Biscay. It is a favorable situation for the entry of Atlantic air masses through the Gulf of Lion to the western Mediterranean Basin allowing to the renewal of air masses and the removal of aerosols that may have accumulated over the Basin (Escudero et al., 2007). Moreover the aerosols are also removed by wet scavenging, which is the strongest removal mechanism (Pruppacher and Klett, 1997), due to the large precipitation amounts.

In summer, the Azores anticyclone is strengthened and its eastern edge enters the western Mediterranean Basin between the Iberian and the Italian peninsulas, whereas thermal lows develop over the Iberian Peninsula and the Sahara region (Millán et al., 1997). The summer months in the region are characterized by the absence of large-scale forcing and the predominance of mesoscale circulations. In particular, as far as the Iberian Peninsula is concerned, the interaction of the sea-land and mountain-induced breezes, the strong orography, the convergence of surface winds from the coastal areas towards the central plateau and the strong levels of subsidence over the western Mediterranean Basin results in the re-circulation of air masses and the consequent ageing and accumulation of pollutants (Millán et al., 1997; Pérez et al., 2004; Sicard et al., 2006). Furthermore, additional factors come into play such as low precipitation, high photochemistry that boosts the formation of secondary organic aerosols, and the increased convective dynamics that favors resuspension. Summer is also a period

favorable to the transport towards the Basin of aerosols such as desert dust from Morocco and western Algeria to the northwestern Mediterranean basin following the SW-NE axis of our stations when Atlantic low pressure systems arrive over Spain (Bergametti et al., 1989; Moulin et al., 1998; Valenzuela et al., 2012a), and forest fire smoke (Bergametti et al., 1992; Guieu et al., 2005; Pace et al., 2005). The summer and annual amount of desert dust exported to the Basin is controlled by the large-scale North Atlantic Oscillation (NAO; Moulin et al., 1997; Papadimas et al., 2008; Pey et al., 2013) which also partly controls the number of fires around the Basin: during period of high NAO index (defined by Hurrel, 1995), drier conditions prevail over southern Europe, the Mediterranean Sea, and northern Africa (Papadimas et al., 2008).

4.2 Peculiarity of each of the three sites

Corsica, where the Ersa site is located, is a North–South elongated French island (~80 × 180 km^2) situated in the northern part of the western Mediterranean Basin. It has the highest mountains (behind Mount Etna) and the largest number of rivers than any Mediterranean island. The highest peak reaches 2710 m and there are about twenty other summits higher than 2000 m. The northern tip of the island is at about 160 km from the coast of southern continental France and at about 80 km from the coast of Italy. The dominant wind directions are W and E-SE (Lambert et al., 2011). The site is perfectly suited for regional background studies since it is not impacted by any type of local anthropogenic aerosol. There are relatively few aerosol measurements over Corsica in the scientific literature at present despite the recurrent high summer pollution peaks and intense rainfalls observed in the island in the last few years (Lambert and Argence, 2008). However, the French scientific community has started the installation of a multi-site instrumented platform, called CORSiCA (Corsican Observatory for Research and Studies on Climate and Atmosphere-ocean environment), dedicated to oceanographic and atmospheric studies in the framework of the HyMeX (Hydrological cycle in the Mediterranean Experiment) and ChArMEx projects (Lambert et al., 2011). Carbonaceous aerosols and dust in a lesser extent were highlighted as the main driver of the aerosol optical properties of surface aerosols at Ersa in summer (Nicolas et al., 2013; Sciare et al., 2014). Carbonaceous aerosols also control the averaged aerosol column properties on a yearly basis in the northwestern basin (Mallet et al., 2013). From MODIS satellite products, Gkikas et al. (2016) report less than 4 episodes per year of strong desert dust episodes (AOD > 0.44, defined as the annual mean + 2 standard deviations) at Ersa in the period 2000-2013.

The island of Mallorca is approximately 2.5 times smaller than Corsica in surface. The mountainous chain of the island, the Sierra de Tramuntana, is situated in the northwestern part

and its highest peak reaches 1445 m. The AERONET sun-photometer is situated at the airport of the capital, Palma de Mallorca (~420,000 inhabitants), approximately 8 km east of the city center and harbor area. The winds are driven by the topographic effects of the Sierra de Tramuntana chain. The dominant wind directions observed close to the city center are SW and NE to which a NW component adds in winter (Pey et al., 2009). There are also relatively few aerosol measurements over Mallorca in the scientific literature. In average 20 % of the days/year are affected by desert dust events (Pey et al., 2009). Carbonaceous aerosols in Mallorca have been found by Pey et al., (2009) in the same range that those in other suburban sites in Spain, which suggests an important regional contribution of carbonaceous aerosols. Gkikas et al. (2016) report an average of almost 6 intense (AOD > 0.50) desert dust episodes per year in the period 2000-2013.

The Alborán island is a tiny (7 ha), totally flat island situated in the Alboran Sea, about 200 km East of the Gibraltar Straight, 50 km north of the Moroccan coast and 90 km south of the Spanish coast. There is no local anthropogenic emission source on and near the island, except for an important shipping route at the north of it (www.marinetraffic.com). The only aerosol measurements ever performed at Alborán are those used in this work. They are extensively discussed in Lyamani et al. (2015) and Valenzuela et al. (2015). During the AERONET measurement period of June 2011 – January 2012, 35 % of the air masses originated on the Atlantic/Iberian Peninsula, 31 % on North Africa, 21 % on the European/Mediterranean region and 13 % were pure maritime aerosols (Lyamani et al., 2015; Valenzuela et al., 2015). During the dust events, Valenzuela et al. (2015) stress that the aerosol properties are clearly different from pure mineral dust and that most of the desert dust intrusions over Alborán can be described as a mixture of dust and anthropogenic fine absorbing particles independently of the dust source area. Gkikas et al. (2016) report an average of almost 10 episodes per year of strong desert dust episodes (AOD > ~0.59) in the period 2000-2013.

5 Seasonal and annual variability of aerosol properties at Ersa and Palma

5.1 AOD, AE and fine mode contribution

The seasonal aerosol classification performed with the methodology described in Section 3 is presented in Figure 2 for Ersa and in Figure 3 for Palma. Seasonal mean values of AE and δAE are given in Table 1. The graphs were made with the whole AOD dataset. We first observe that in winter at both sites the criteria $AOD_{675} > 0.15$ removes a lot of points and results in a poor statistics (N=24 at Ersa and N=4 at Palma). As discussed further in this Section, we

believe that the statistics in spring at Palma is not totally representative of the site: N=68 is rather low and no point with $AOD_{440} > 0.4$ is found (Figure 3d), whereas at Ersa many points do have $AOD_{440} > 0.4$ (Figure 2d). For the rest of the seasons, moderate to large AODs ($AOD_{440} > 0.4$) gather in two well differentiated cluster. In summer Ersa and Palma present an important fine mode cluster ($AE > 1.4$; $\delta AE < 0$ and $AE > 1.2$; $\delta AE < 0.2$, respectively) associated to ($70 < \eta < 90$ %; $0.10 < r^f < 0.15$ μm) and ($\eta > 60$ %; $0.10 < r^f < 0.18$ μm), respectively, and corresponding to polluted and continental air masses. At both sites the AOD_{440} increase observed is associated to an increase of the fine mode radius and of the fine mode fraction. The same behavior has been observed in the western Mediterranean Basin by Basart et al. (2009) and was attributed to an increase of r^f following coagulation-aging and hydration of fine particles (Titos et al., 2014; Granados-Muñoz et al., 2015). In this fine mode cluster the largest AODs are logically found at Ersa which is closer to the European continent than Palma. At the same time coarse particles, likely maritime aerosols, superimpose their signal onto this fine mode. A concurrent increase in AOD_{440} and coarse mode fraction along the r^f curves (between 0.10 and 0.12 μm) and for $\eta < 70$ % is observed. During the same summer season both sites also present an important coarse mode cluster ($AE < 0.7$; $-0.1 < \delta AE < 0.2$ and $AE < 0.7$; $0 < \delta AE < 0.4$, respectively) associated to $\eta < 40$ % at both sites and corresponding to mineral dust. In this coarse mode cluster the largest AODs are logically found at Palma which is closer to the African continent than Ersa. The AOD increase is linked to a decrease of δAE towards 0 which is related to almost pure mineral dust as observed in Sub-Sahelian sites (Basart et al., 2009). The points of this coarse mode cluster for which δAE exhibits positive values indicate the presence of small particles mixed with this coarse mode. The difference between the summer mean values of AE (larger at Ersa than at Palma; 1.46 vs. 1.14) and δAE (lower at Ersa than at Palma; 0.05 vs. 0.29) given in Table 1 reflect the general trends found from Figure 2a and Figure 3a. In autumn the frequency of moderate to large AOD events decreases at both sites compared to summer. Both fine and coarse mode clusters are also present but with less variability. The fine mode cluster at Ersa and Palma is marked by ($AE > 1.4$; $\delta AE < -0.2$) and ($AE > 1.5$; $\delta AE < 0.0$), respectively, and is associated to ($70 < \eta < 95$ %; $0.11 < r^f < 0.15$ μm) and ($70 < \eta < 90$ %; $0.10 < r^f < 0.14$ μm), while the coarse mode cluster is marked by ($AE < 0.7$; $\delta AE < 0.3$) and ($AE < 0.5$; $\delta AE < 0.3$) and is associated to $\eta < 30$ and $\eta < 20$ %. The spring plot for Ersa (Figure 2d) is similar to that of summer but with less occurrences. The most interesting differences are a greater number of high-AOD ($AOD_{440} > 0.6$) dust events (coarse mode cluster) in spring compared to summer and conversely a greater number of high-AOD ($AOD_{440} > 0.6$) pollution events (fine mode cluster) in summer compared to spring. In the five-

year period 2011-2015 Ersa has at least three full years of data, while Palma has more sparse data. Before starting with the monthly analysis, the representativeness of Palma data is checked with Ersa data by taking the subset of Ersa data coincident in time with those of Palma (which are comprised in the period August 2011 – December 2013). In Figure 4a the monthly means of this restricted dataset (black bullets) are superimposed on the monthly means of the whole dataset (red bullets). In all cases the monthly means of the 08/11–12/13 dataset are within the monthly variability of the whole dataset. In summer and autumn, the representativeness of the 08/11 – 12/13 dataset is good: the difference between both datasets is lower than 0.01. The highest differences, 0.02 – 0.04, are reached during the period February–May. In the Palma restricted dataset only spring 2013 contributes to the spring mean. Curiously during that spring no moderate to large AODs (AOD_{440} > 0.4) were observed (see Figure 3d). This result may produce the underestimation of the 08/11 – 12/13 dataset compared to the whole dataset observed at Ersa in March and April and suggests that Palma monthly means during those months may also be underestimated. Given the restriction of the Palma dataset, the discussion of the Palma spring means has to be taken cautiously in the following.

The monthly mean AOD_{440} shows a clear annual cycle at Ersa and Palma (Figure 4a). Maxima of 0.22 at Ersa and 0.25 at Palma are observed in July. Those maxima are due to a combination of mineral dust outbreaks and pollution events at Ersa and mostly to mineral dust outbreaks at Palma (see the seasonal aerosol frequency and classification in Section 5.3). The decreasing trend in AOD during the autumn months (from September to November) is identical at both sites. The AOD in spring is lower at Palma than at Ersa, while it is the opposite in summer/autumn. The background AOD in spring at Ersa is dominated by small particles located in the marine boundary layer, present throughout the year (Sciare et al., 2014), while at Palma the predominance of the Atlantic advection meteorological scenario in spring leads to the renovation of air masses at regional scale through the Gulf of Lion and to the cleaning of the atmosphere (Escudero et al., 2007). The summer mean AOD_{440} (± standard deviation) is 0.19±0.10 and 0.23±0.12 at Ersa and Palma, respectively, while the winter averages vary between 0.07 and 0.08.

In order to see the contribution of the fine mode particles we have plotted the fine mode AOD_{440}, AOD^{f}_{440}, in Figure 4b. Except for two months (March and April) the annual cycles at both Ersa and Palma are similar in shape and magnitude. Similar maxima are found in summer (0.13±0.09 at Ersa and 0.12±0.07 at Palma). In March and April AOD^{f}_{440} is more than double at Ersa than at Palma. In addition to the possible underestimation of the Palma dataset in spring

(see two paragraphs above), the maps of AOD per aerosol type from Barnaba and Gobbi (2004) suggest a contribution of aerosols of continental origin already in spring over Corsica and not before summer over the Balearic Islands. We cannot confirm this result with the (δAE, AE) plots because of the limited representativeness of Palma data during the spring months.

The monthly $AE_{440–870}$ plot (Figure 4c) shows different seasonal patterns at both sites. At Ersa it slightly increases in spring/summer and reaches a maximum value of 1.50 in September. At Palma, it oscillates between 0.84 (March) and 1.34 (September) without any significant seasonal trend. The higher values at Ersa compared to Palma indicate the presence of finer particles at Ersa throughout the year. The $AE_{440–870}$ annual means at Ersa and Palma are 1.37±0.47 and 1.14±0.46, respectively, with maxima in summer (1.46±0.45 and 1.14±0.47, respectively). The coarse mode fraction (not shown, see Sicard et al., 2014) looks reversely correlated to the AE: it decreases at Ersa in spring/summer and reaches a minimum in July, while no marked trend is observed at Palma. The fact that $AE_{440–870}$ is lower in spring than in summer at Ersa reflects the higher frequency of dust events in spring compared to summer as found earlier from our aerosol classification.

5.2 Volume size distribution

Figure 5 shows the seasonal variability of the aerosol particle size distribution at both sites. Seasonal mean values are given in Table 1 for (r_V^f, C_V^f) and (r_V^c, C_V^c), the volume median radius and the volume concentration of the fine and coarse modes, respectively. The annual volume concentration values (varying between 0.017 and 0.021 $\mu m^3 \cdot \mu m^{-2}$ for the fine mode and between 0.027 and 0.046 $\mu m^3 \cdot \mu m^{-2}$ for the coarse mode) at both sites are typical of maritime (Smirnov et al., 2002) and/or background/rural (Omar et al., 2005) environments. The annual values at Palma are very similar to the mean size distribution averaged over several sites in the western Mediterranean Basin by Mallet et al. (2013). The winter fine mode volume concentrations are similar at both sites (~ 0.010 $\mu m^3 \cdot \mu m^{-2}$). In spring the fine mode volume concentration more than doubles (w.r.t. winter) at Ersa while it is stable at Palma. This behavior is reflected on AOD_{440}^f (Figure 4b) which doubles from winter to spring at Ersa because of the contribution of aerosols of continental origin already in spring over Corsica and not before summer over the Balearic Islands. The domination of large particles (mostly mineral dust) is particularly remarkable during the summer period at both sites. Relatively large coarse mode concentrations are also visible in spring at Ersa and in autumn at Palma. A clear summer inter-site difference is observed on the coarse mode volume concentration (0.032±0.036 at Ersa vs.

0.063±0.063 at Palma) and also on the C_V^c / C_V^f ratio (1.7 vs. 2.5, respectively). The summer coarse mode volume median radii (2.49±0.41 and 2.43±0.41) fall in the range of values for dusty sites (1.90 – 2.54 μm; Dubovik et al., 2002b) and are in agreement with the average value of 2.34 μm found for the western Mediterranean Basin by Mallet et al. (2013). As commented by Dubovik et al. (2002b) the absence of dynamics between the particle radius and the aerosol loading explains that dust median radii are smaller than those of urban/industrial aerosols. The influence of European pollution decreases from Ersa to Palma and, logically, the coarse mode volume median radius decreases. In the same line, we also observe that inter-season r_V^c decreases with increasing mineral dust frequency (see the seasonal aerosol frequency and classification in Section 5.3).

5.3 AAOD, absorption Ångström exponent and refractive index

Besides aerosol amount and size, other important aerosol properties are those related to their absorpting ability. It must be kept in mind that AERONET level 2.0 inversion products linked to the aerosol absorption properties like the aerosol absorption optical depth, the absorption Ångström exponent (AAE) and the refractive index are performed with the following restrictions: 50 < SZA < 80º and AOD_{440} > 0.4. To gain an insight into the seasonal frequency, intensity and aerosol type under such restrictions, we show in Figure 6 the (δAE, AE) plots only for those AERONET level 2.0 inversion products in our dataset that meet those criteria. There is in general twice more data available in summer than in the other seasons. The plots for both sites show without ambiguity that such restrictions lead to only two types of aerosols: mineral dust corresponding to the coarse mode cluster (δAE < 0.3; $AE_{440\text{-}870}$ < 0.75; η < 40%) and pollution corresponding to the fine mode cluster ($AE_{440\text{-}870}$ > 1.0; η > 70%). The seasonal number and ratio of each of these two aerosol types and their respective seasonal mean AOD_{440} are given in Table 2. In summer 58 % (84 %) of the measurements correspond to mineral dust at Ersa (Palma) and 42 % (16 %) to pollution. In autumn the predominance is opposite: 33 % (40 %) of the measurements correspond to mineral dust at Ersa (Palma) and 67 % (40 %) to pollution. In spring at Ersa 64 % of the measurements correspond to mineral dust and 36 % to pollution. The seasonal mean AOD_{440} for pollution is quite constant (~0.46 – 0.47) and has negligible inter-site and inter-season variations, which suggests that the intensity of pollution events is quite uniform over the western Mediterranean Basin. The seasonal mean AOD_{440} for mineral dust (MD) is more variable (higher standard deviations). The higher annual AOD_{440} values found at Ersa (0.55) vs. Palma (0.51) suggest that a significant number of MD events with 0.40 < AOD_{440} < 0.50 detected at Palma do not reach Ersa. The limitation of the graphical

method used here is that no information related to the aerosol absorption properties is retrieved. In the following we will try to link the dominant aerosol size, type and frequency found with the absorption properties.

Bergstrom et al. (2007) report that the spectral AAOD for aerosols representing the major absorbing aerosol types (pollution, biomass burning, desert dust and mixtures) decreases with wavelength and can be approximated with a power-law wavelength dependence, the absorption Ångström exponent which can be calculated between two wavelengths λ_1 and λ_2, $AAE_{\lambda_1-\lambda_2}$, as:

$$AAE_{\lambda_1-\lambda_2} = -\frac{\ln\left[\frac{AAOD_{\lambda_1}}{AAOD_{\lambda_2}}\right]}{\ln\left[\frac{\lambda_1}{\lambda_2}\right]} \quad (2)$$

The range of values of AAE provides useful information on shortwave absorption produced by different types of aerosols, namely black carbon (BC), organic carbonaceous matter, and mineral dust (Russell et al., 2010). However, recently, Mallet et al. (2013) highlighted the difficulties in attributing AAE values larger than 1, the value for pure BC, to organic species (and/or mineral dust) or to coated BC since they all produce AAE > 1 (Lack and Cappa, 2010).

The seasonal variations of the spectral dependency of the aerosol absorption optical depth are shown in Figure 7a. Seasonal mean values are given in Table 1. At each site the spectra are shown for the whole dataset (All) and for mineral dust (MD) and pollution (Pol) cases determined with the classification obtained from Figure 6 (see first paragraph of this Section). In both Ersa and Palma the AAOD decreases with increasing wavelength. The annual $AAOD_{440}$ is 0.023±0.018 at Ersa and 0.040±0.020 at Palma. The associated $AAE_{440\text{-}870}$ is 1.66±0.66 and 1.88±0.53, respectively. The spectra of AAOD for pollution are quite similar in shape and magnitude at both sites and present weak inter-season variations. It is rather low (< 0.02) with low spectral dependency (AAE oscillates between 1.10 and 1.24) and is slightly higher at Palma than at Ersa. The mineral dust AAOD ($0.023 < AAOD_{440} < 0.057$) and AAE ($1.43 < AAE < 2.69$) are much higher than those for pollution and present larger inter-season and inter-site variations. At Ersa in spring $AAOD_{440}$ (AAE) reaches its highest value, 0.035 (2.11), when the mineral dust outbreaks represent 64 % (the highest percentage) of the cases. At Palma the highest values of $AAOD_{440}$ (AAE), 0.043 (1.98), occur in summer also when the mineral dust outbreaks are the most frequent (84 %). The summetime average of $AAOD_{440}$ at Ersa (0.018) measured over the whole dataset is within the error bar of the value found by Mishra et al. (2014; 0.020) at the same site from a larger dataset of AERONET observations. It is however

lower than the average value given in Mallet et al. (2013) for the western Mediterranean Basin calculated at sites characterized mostly as urban and dusty, which could indicate that they considered more dusty sites than urban ones in the computing of their basin average. The mineral dust AAOD spectra at both sites are similar in magnitude and shape to the measurements made during PRIDE (Puerto Rico Dust Experiment, 2000; aerosols: Saharan dust) and ACE-Asia (Aerosol Characterization Experiment-Asia, 2001; aerosols: Asian dust, urban and industrialized) (Bergstrom et al., 2007; Russell et al., 2010). The pollution and MD AAE found here are in agreement with the mean values observed at several Mediterranean AERONET sites for urban sites (1.31) and dusty sites (1.96), respectively (Mallet et al., 2013). The annual mean values of AAE (1.66 and 1.88 at Ersa and Palma, respectively) fall within the range 1.5 – 2, in which the AAE at different wavelength pairs vary at the dusty site of Solar Village, Saudi Arabia (Russell et al., 2010). It results that on a yearly basis AAE is strongly influenced by mineral dust outbreaks, even at Ersa.

The seasonal spectral variations of the real and the imaginary part of the refractive index (RRI and IRI, respectively) are shown in Figure 7b and Figure 7c. Seasonal mean values at 440 nm (RRI_{440} and IRI_{440}) are given in Table 1. Figure 7b shows a large inter-season and inter-site variability in the shape and amplitude of the RRI spectra. RRI_{440} has an annual mean value of 1.45±0.04 at Ersa and 1.43±0.06 at Palma. These values are on the order of magnitude of those found by Mallet et al. (2013) from AERONET observations at various sites around the Mediterranean Basin and they are in the upper limit of urban/industrial aerosols (1.33 – 1.45) and lower than "pure" dust (1.48 – 1.56; Dubovik et al., 2002b). However the values significantly differ by aerosol type: $1.38 < RRI_{440} < 1.45$ and $1.45 < RRI_{440} < 1.55$ for pollution and mineral dust, respectively, agreeing well with the results from Dubovik et al. (2002b). The high variability of RRI_{440} for mineral dust is probably linked to variations in the dust mineralogy. RRI spectra are nearly constant for pollution. For mineral dust RRI shows in all cases a decrease of ~ 0.02 – 0.04 towards ultraviolet wavelengths, whereas Petzold et al. (2009) determined wavelength-independent RRI from airborne measurements of dust during the SAMUM (Saharan Mineral Dust Experiment) campaign. This difference may be due to differences in the measurement techniques, but also in a wrong mixture of spherical and non-spherical in the AERONET product. Indeed Dubovik et al. (2000b; 2002a) showed that treating non-spherical particles (like mineral dust) like spheres result in an erroneous decrease of RRI with decreasing wavelength. The values of RRI_{440} for MD are in agreement with previous works such as Petzold et al. (2009) who found 1.55 – 1.56 at 450 nm for dust during SAMUM and Denjean et al. (2016) who found 1.50 – 1.55 at 530 nm in dust layers from airborne

measurements over the western Mediterranean Basin during the ChArMEx 2013 field campaign.

IRI_{440} (Figure 7c) has an annual mean value of $(3.1\pm1.3) \times 10^{-3}$ at Ersa and $(4.7\pm1.8) \times 10^{-3}$ at Palma. The annual IRI_{440} are in the lower limit of the values found from AERONET observations by Mallet et al. (2013) at various sites around the Mediterranean Basin (3.5-11.9 $\times 10^{-3}$) where the minimum (3.5×10^{-3}) was observed at the Italian Island of Lampedusa. Although we previously found that $AAOD_{440}$ was higher for MD than for pollution, the reverse occurs for IRI_{440} which is in general higher for pollution than for MD. This result indicates that these larger MD AAOD values are the result of larger amounts of MD (compared to pollution) in terms of optical depth and not of MD intrinsic absorption properties. IRI_{440} varies in the range $(2.3 – 4.9)$ and $(3.0 – 5.1) \times 10^{-3}$ for MD and pollution, respectively, and in general larger values are found at Palma. While the pollution spectrum of IRI is nearly wavelength-independent, that of MD shows a strong increase towards ultraviolet wavelengths. As the imaginary part of the refractive index is driven by iron oxide content (especially hematite), it results in a higher IRI at shorter wavelengths during episodes with high dust concentrations (Moosmüller et al., 2009). The ranges of IRI_{440} found for pollution and MD are in agreement with previous works: during the TARFOX (Tropospheric Aerosol Radiative Forcing Observational Experiment) campaign in 1996 values of $(1 – 8) \times 10^{-3}$ were found off the US Atlantic coast in horizontal layers of distinct aerosol refractive indices using a retrieval based on aerosol in-situ size distribution and remote sensing measurements (Redemann et al., 2000); during SAMUM Petzold et al. (2009) retrieved values of desert dust IRI at 450 nm of $(3.1 – 5.2) \times 10^{-3}$; Denjean et al. (2016) found values of IRI at 530 nm between 0 and 5×10^{-3} at different heights in dust layers during the ChArMEx 2013 field campaign.

5.4 Single scattering albedo and asymmetry factor

The single scattering albedo (SSA) is the ratio of aerosol scattering to total extinction (i.e. scattering + absorption) that provides some information on the aerosol absorption properties. It is useful to relate the AAOD to the AOD:

$$AAOD_{\lambda} = \left(1 - SSA_{\lambda}\right) AOD_{\lambda} \quad (3)$$

The asymmetry factor (g) represents a measure of the preferred scattering direction and varies between -1 (only backward-scattering, i.e. at 180 º relative to the incident direction) and +1 (only forward-scattering at 0º). The SSA and asymmetry factor are of special interest for radiative transfer studies. The seasonal spectral variations of SSA and g are shown in Figure

8. Seasonal mean values at 440 nm (SSA_{440} and g_{440}) are given in Table 3. In average both sites appear as "moderately" absorbing with annual SSA_{440} varying between 0.92±0.03 and 0.96±0.02, even though minima are observed around 0.89 and 0.86 at Ersa and Palma, respectively. In agreement with our previous results (higher $AAOD_{440}$ at Palma than at Ersa) we find lower SSA at Palma compared to Ersa at all wavelengths but especially at 440 nm. MD and pollution SSA spectra have very distinct behaviors: while the first ones increase with increasing wavelength, the second decrease. This result is in agreement with the climatological SSA spectra obtained worldwide by Dubovik et al. (2002b) and plotted by Russell et al. (2010) which shows that SSA_λ decreases with increasing wavelengths for urban/industrial aerosols and biomass burning, and conversely increases with increasing wavelengths for desert dust. During summer, autumn and spring at Ersa and autumn at Palma, the seasonal mean of SSA_λ calculated with the whole dataset (MD + pollution) increases from 440 to 675 nm and decreases afterwards. This behavior is representative of a mixture of both MD and pollution. During summer at Palma the SSA spectra (calculated with the whole dataset) are very similar to that of MD (84 % of the dataset corresponds to mineral dust, see Table 2). MD and pollution SSA_{440} vary in the range 0.89 – 0.95 and 0.97 – 0.98, respectively. For comparison Denjean et al. (2016) found SSA at 530 nm ranging from 0.90 to 1.00 in layers of different aerosol types in the western Mediterranean Basin during the ChArMEx 2013 field campaign. Inter-season variations are more pronounced for MD than for pollution. As a consequence of higher MD $AAOD_{440}$ in autumn, MD SSA_{440} is smaller in autumn than in summer.

The annual mean values of the asymmetry factor at 440 nm (g_{440}) are 0.69±0.03 and 0.70±0.03 at Ersa and Palma, respectively. The mean values of both pollution and MD g_{440} show very little inter-season and inter-site variations: they range between 0.68 and 0.70, and between 0.71 and 0.73, respectively. Figure 8b shows that the spectra of g have a general tendency to decrease with increasing wavelengths for pollution, while it is nearly constant for MD. These results are in agreement with the climatology from Dubovik et al. (2002b) who found similar g_{440} for urban/industrial aerosols and desert dust (0.68 – 0.73) and a decreasing tendency with increasing wavelength for urban/industrial aerosols. Lyamani et al. (2006) who compared the asymmetry factor spectra at Granada for dust events and urban/industrial aerosols (European contamination) also found that the decrease of the g spectra with increasing wavelengths is much stronger for urban/industrial aerosols than for mineral dust. This result implies that at near-infrared wavelengths ($\lambda > 670$ nm), constant AOD and low SZA the solar radiation scattered to the surface is greater for mineral dust than for urban/industrial aerosols. Here again

the seasonal means calculated with the whole dataset (MD + pollution) have the signature of neither MD, nor pollution, but are representative of a mixture of both MD and pollution.

6 Solar direct radiative forcing and forcing efficiency at Ersa and Palma

The AERONET Version 2.0 retrieval provides a set of radiative quantities in the solar (so called shortwave) spectrum range including spectral downward and upward total fluxes at the surface, diffuse fluxes at the surface, and broadband upward and downward fluxes as well as aerosol radiative forcing (ARF) and aerosol radiative forcing efficiency (ARFE) both at the bottom of atmosphere (BOA) and at the top of the atmosphere (TOA). The radiative forcing accounts for changes in the solar radiation levels due to changes in the atmospheric constituents. The direct radiative forcing of atmospheric aerosols is defined as the difference in the energy levels between two situations with and without aerosols:

$$ARF_{BOA} = \Delta F^{w}_{BOA} - \Delta F^{o}_{BOA} \quad (4)$$

$$ARF_{TOA} = \Delta F^{w}_{TOA} - \Delta F^{o}_{TOA} \quad (5)$$

where ΔF^{w} and ΔF^{o} are the downward net (downwelling minus upwelling) fluxes with and without aerosols, respectively. With this convention, a negative sign of the ARF implies an aerosol cooling effect and a positive sign an aerosol warming effect, regardless of whether it happens at the BOA or at the TOA. The ARFE is defined as the ratio of ARF per unit of AOD. The ARF analytical definitions used by AERONET (AERONET, 2016) are slightly different than Eqs. (4) and (5):

$$ARF^{AER}_{BOA} = F^{w\downarrow}_{BOA} - F^{o\downarrow}_{BOA} \quad (6)$$

$$ARF^{AER}_{TOA} = F^{0\uparrow}_{TOA} - F^{w\uparrow}_{TOA} \quad (7)$$

While Eq. (7) is equivalent to Eq. (5) because the downwelling flux at the TOA is independent of the presence or not of aerosols in the atmosphere ($F^{w\downarrow}_{TOA} = F^{o\downarrow}_{TOA}$), the use of Eq. (6) yields an overestimation w.r.t. the real value since the upward fluxes with and without aerosols are not taken into account.

In the AERONET retrieval approach, the flux calculations account for the thermal emission, absorption and single and multiple scattering effects using the Discrete Ordinates Radiative Transfer (DISORT) method (Stamnes et al., 1988). The solar broadband fluxes are calculated for SZA between 50 and 80°, by spectral integration in the range from 0.2 to 4.0 μm. The integration of atmospheric gaseous absorption and molecular scattering effects are conducted using the Global Atmospheric Model (GAME) code (Dubuisson et al., 1996; 2004; 2006). It is

worth noting that flux calculations are performed for a multi-layered atmosphere with a gaseous vertical distribution calculated with the US standard atmosphere model and a single fixed aerosol vertical distribution (exponential decrease with aerosols up to a height of 1 km). García et al. (2008) tested different vertical profiles and their sensitivity tests led to differences of less than 1 $W \cdot m^{-2}$ on the downward solar flux at the BOA and estimated those differences (~ 0.2 – 3 % w.r.t. the instantaneous ARF) negligible. Detailed information on the radiative transfer module used by the operational AERONET inversion algorithm can be found in García et al. (2011; 2012a; 2012b).

García et al. (2008) made an intensive validation of AERONET estimations of fluxes and radiative forcings using ground-based measurements from solar databases at 9 stations worldwide but AERONET estimations of the aerosol direct radiative forcing are little used in the literature. Cachorro et al. (2008) used the AERONET ARF estimations to study the impact of an extremely strong desert dust intrusion over the Iberian Peninsula. Derimian et al. (2008) used the AERONET estimates of the ARF for mineral dust mixed with biomass burning and for pure mineral dust at M'Bour, Senegal, and tested the impact of neglecting aerosol non-sphericity on radiative effect calculations. García et al. (2011) did a similar work but at regional level for mixtures of mineral dust and biomass burning and mineral dust and urban/industrial aerosols. Valenzuela et al. (2012b) checked AERONET estimates of the radiative fluxes against SBDART (Santa Barbara DISORT Atmospheric Radiative Transfer; Ricchiazzi et al., 1998) computations for desert dust events affecting the Southeastern Iberian Peninsula. García et al. (2012a; 2012b) have used AERONET estimates of the ARF at 40 stations grouped in 14 regions worldwide for six aerosol types: mineral dust, biomass burning, urban/industrial, continental background, oceanic and the free troposphere.

6.1 Validation of AERONET radiative fluxes with ground-based and satellite data

In order to validate AERONET estimations of the solar fluxes at our western Mediterranean stations, we have performed a comparison of the fluxes the most critical for aerosol forcing calculations, namely:

- The solar downward flux at the surface, $F_{BOA}^{\downarrow}$. We have performed a comparison between AERONET estimations and pyranometer measurements, using the Barcelona AERONET / SolRad-Net (Solar Radiation Network, http://solrad-net.gsfc.nasa.gov/) site which is the closest site to our study area in the western Mediterranean Basin where collocated AERONET and solar flux measurements are available. The period with

coincident measurements is May 2009 – October 2014. The pyranometer is a Kipp and Zonen CMP21 sensor that provides every two minutes a measurement of the total solar flux in the range 0.3–2.8 μm. Coincident AERONET and pyranometer measurement times were restricted to ± 1 min. We used SolRad-Net level 1.5 data which have been cleared of any operational problem The manufacturer accuracy (2 %) and the sensor drift (< 1 %) yield an overall accuracy on the order of 3%.

- The solar upward flux at the TOA, $F_{TOA}^{\uparrow}$. We have performed a comparison between AERONET estimations and CERES (Clouds and the Earth's Radiant Energy System) satellite measurements at Ersa, Palma and Alborán. We used CERES Single Scanner Footprint (SSF) Level 2 products, namely the shortwave (0–5 μm) upward flux at the TOA given for a spatial resolution equivalent to its instantaneous footprint (nadir resolution 20-km equivalent diameter). Measurements from CERES/Aqua and CERES/Terra were used indistinctively. We screened CERES data spatially by accounting only for the pixels in which one of the ground sites falls, and temporally allowing a time difference of ± 15 min. The time of overpass of both CERES/Aqua and CERES/Terra over the three sites varies in the range 10–14 UT. The CERES/Terra instantaneous shortwave TOA flux uncertainties are estimated to be 13.5 $W \cdot m^{-2}$ for all-sky conditions (CERES, 2016). According to Loeb et al. (2007) CERES/Aqua TOA flux errors are similar to those of CERES/Terra. Because of the CERES overpass time range (10–14 UT) the SZA restriction for AERONET level 2.0 data (50 < SZA < 80º) rejects many measurements that coincide in time but are for SZA < 50º. Consequently the use of AERONET level 2.0 data provides very few points for comparison. We have therefore selected AERONET level 1.5 data with 40 < SZA < 80º and checked that the cases with 40 < SZA < 50º represent ~ 33 % of the total. We had to deal with two more issues to further filter CERES data points: 1) sometimes CERES pixels are affected by clouds when at the coincident time AERONET is not, and 2) because the three sites are in coastline regions CERES pixels contain information from both land and water. The first issue is due to the different techniques used by both AERONET sun-photometers and CERES which make the air mass volumes sampled by both instruments quite different. The second one is in general not problematic, except at given periods of the year and at given hours of the day when the sun glint produces a significant increment of the upward fluxes in the direction of the spaceborne sensor. Both cases result in an increase of CERES upward fluxes at the TOA. To discard those cases, we eliminated from the comparison all pairs of points (CERES, AERONET) that have a difference

larger than CERES uncertainty, i.e. 13.5 W·m^{-2}. The AERONET level 1.5 data are from 2008–2014 at Ersa, 2011–2014 at Palma and 2011–2012 at Alborán.

Figure 9a shows the comparison of downward solar fluxes at the BOA measured by pyranometers vs. that estimated by AERONET. A very good agreement is found between both quantities (correlation coefficient, R, greater than 0.99). To quantify the level of accuracy we calculated the average difference between the AERONET modeled and observed flux. We found +12 W·m^{-2} which, in relative terms, corresponds to an overestimation of AERONET fluxes of +3.0 %, increment found by dividing the average AERONET modeled flux by the observed one. This value is in the range of mean relative errors [-0.6, +8.5 %] found by García et al. (2008) under different aerosol environments at 9 stations worldwide. Derimian et al. (2008) found an overestimation of approximately +4 % in M'Bour, Senegal. According to García et al. (2008) that overestimation is due mostly to the cosine effect (the pyranometer angular response which can deviate up to ± 3 % from the truth at SZA of 70-80º) and to the surface albedo and bidirectional reflectance distribution function (BRDF) assumed by AERONET. The least-square fit linear equation relating the AERONET (AER) fluxes to the observation (OBS) is $OBS = 0.98 \cdot AER - 4.50$. Our results are in total agreement with García et al. (2008) who found $OBS = 0.98 \cdot AER - 5.32$. Since the validation of $F_{BOA}^{\downarrow}$ has been performed regardless of the aerosol load, we can easily assume that the fluxes with turbid (high aerosol load) or clean (low aerosol load) atmospheres follow the same regression line ($OBS = 0.98 \cdot AER - 4.50$). Finally, to correct for the missing upward fluxes in the definition of ARF_{BOA}^{AER}, the latter can be multiplied by the term (1 – SA) where SA stands for the surface albedo. Indeed:

$$\begin{aligned} ARF_{BOA} &= \Delta F_{BOA}^{w} - \Delta F_{BOA}^{o} \\ &= \left(F_{BOA}^{w\downarrow} - F_{BOA}^{w\uparrow}\right) - \left(F_{BOA}^{o\downarrow} - F_{BOA}^{o\uparrow}\right) \\ &= \left(F_{BOA}^{w\downarrow} - SA \cdot F_{BOA}^{w\downarrow}\right) - \left(F_{BOA}^{o\downarrow} - SA \cdot F_{BOA}^{o\downarrow}\right) \\ &= \left(F_{BOA}^{w\downarrow} - F_{BOA}^{o\downarrow}\right)\left(1 - SA\right) \end{aligned} \tag{8}$$

Consequently the corrected estimated solar ARF at the BOA, ARF_{BOA}^{c} in W·m^{-2}, has been calculated from the original AERONET radiative forcing, ARF_{BOA}^{AER}, as:

$$ARF_{BOA}^{c} = 0.98 \cdot ARF_{BOA}^{AER} \cdot \left(1 - SA\right) \tag{9}$$

The term 0.98 comes from the correction of the fluxes after comparison to pyranometer measurements. We have considered a broadband value of SA calculated as the average of the

surface albedo at the four AERONET wavelengths (440, 675, 870 and 1020 nm). García et al. (2012b) document that considering the surface albedo at the four AERONET wavelengths yields differences less than 10 % w.r.t. considering spectral surface albedo in the whole solar spectral range (0.2 – 4.0 μm). The corrected solar ARFE at the BOA, $ARFE^{c}_{BOA}$ in W·m^{-2}·AOD$^{-1}_{550}$, defined here as the ratio of forcing per unit of AOD at 550 nm, can be simply calculated from the original AERONET ARFE, $ARFE^{AER}_{BOA}$, as:

$$ARFE^{c}_{BOA} = 0.98 \cdot ARFE^{AER}_{BOA} \cdot (1 - SA) \quad (10)$$

Figure 9b shows the comparison of upward solar fluxes at the TOA measured by CERES vs. estimated by AERONET. The pairs of point (open bullets) outside the shaded area representing CERES uncertainty, 13.5 W·m^{-2}, were not taken into account in the fit and are reported only for completeness. One sees that almost all of these points are on the upper side of the diagonal indicating an underestimation by AERONET estimates probably due to an increment of the upward fluxes in the direction of the spaceborne sensor caused by clouds or sun glint. Here again, but in a lesser extent compared to the validation of $F^{\downarrow}_{BOA}$, the pairs of points taken into account in the fit calculation (solid color bullets) show a good agreement between both AERONET modeled and observed fluxes (R > 0.92). The average difference between the AERONET modeled and observed flux is -1.5 W·m^{-2} which, in relative terms, corresponds to an underestimation of AERONET fluxes of -1.6 %. To our knowledge it is the first time that AERONET fluxes at the TOA are validated with satellite measurements. The least-square fit linear equation relating the AERONET (AER) fluxes to the observation (OBS) is $OBS = 0.99 \cdot AER + 2.51$. Like at the BOA, since the validation of $F^{\uparrow}_{TOA}$ has been performed regardless of the aerosol load, the correction of the fluxes can be assumed the same for atmospheres with and without aerosols. Then the corrected ARF at the TOA, ARF^{c}_{TOA}, and the corrected ARFE at the TOA, $ARFE^{c}_{TOA}$, write:

$$ARF^{c}_{TOA} = 0.99 \cdot ARF^{AER}_{TOA} \quad (11)$$

$$ARFE^{c}_{TOA} = 0.99 \cdot ARFE^{AER}_{TOA} \quad (12)$$

6.2 Solar direct radiative forcing and forcing efficiency: monthly variations at Ersa and Palma

The monthly means of the corrected AERONET level 2.0 instantaneous solar ARF and ARFE are shown in Figure 10 at both the BOA and TOA. By plotting the whole dataset of ARF and

ARFE as a function of SZA we have observed that both quantities remained approximately constant independently of SZA. However as SZA increases, the slant path increases and it is logical to expect a decrease of the ARF / ARFE related to the decrease of the solar radiation reaching the Earth. This effect has been observed on instantaneous ARFE observations by Di Sarra et al. (2008) and Di Biagio et al (2009), among others. We therefore decided to filter Figure 10 for SZA $\leq 60^{\circ}$.

The solar ARF is strictly negative and shows a marked annual cycle (at both the BOA and the TOA) at both Ersa and Palma. The solar ARF is lower (in absolute value) during the winter months and reaches maxima (in absolute value) in spring or summer. At the BOA, a maximum (in absolute value) of -20.6 $W \cdot m^{-2}$ is reached at Ersa in March (with a seasonal maximum of -18.0 $W \cdot m^{-2}$ in spring) while the strongest forcing at Palma, -26.4 $W \cdot m^{-2}$, is reached in June (with a seasonal maximum of -22.8 $W \cdot m^{-2}$ in summer). These maxima correspond to the season with the maximum occurrences of mineral dust outbreaks at each site (64 % at Ersa in spring and 84 % at Palma in summer, see Table 2). During the first months of the year (until April) ARF is more than double at Ersa than at Palma. It reflects a similar result found earlier on AOD_{440}^{f} (see Section 5.1 and Figure 4) and may be attributed to 1) the contribution of aerosols of continental European origin already in spring over Corsica and not before summer over the Balearic Islands, hence a higher amount of small particles that causes more cooling (Tegen and Lacis, 1996), and 2) the lack of representative measurements during the spring season at Palma (see Section 5.1). The marked peak in July at Palma (correlated with a peak in AOD_{440}, see Figure 4a) is clearly due to mineral dust outbreaks which are more frequent in summer (see Section 5.3). Another effect sums up: in summer $AAOD_{440}$ (Figure 7) is more than double at Palma (0.043; $SSA_{440} \sim 0.92$) than at Ersa (0.018; $SSA_{440} \sim 0.96$) in summer. According to Boucher and Tanré (2000), the surface forcing is enhanced when the aerosol absorption is larger. At the TOA, the seasonal cycles are similar at both sites. Maxima (in absolute value) are reached during the same season, summer, and the same month, July. The July and summer means are, respectively, -14.5 and -12.8 $W \cdot m^{-2}$ at Ersa and -13.9 and -13.0 $W \cdot m^{-2}$ at Palma. The same difference observed on ARF_{BOA} during the first months of the year is also visible on ARF_{TOA}: ARF_{TOA} at Ersa is almost double (in absolute value) that at Palma; whereas the stronger influence of the dust outbreaks at Palma (vs. Ersa) on ARF_{BOA} during the summer months is not visible at the TOA. This seems to indicate that ARF_{TOA} is not as much affected by dust long-range transport as it is by long-range transport of small particles of continental origin. As far

as aerosol absorption is concerned, Boucher and Tanré (2000) showed that increasing the aerosol absorption decreases the aerosol effect at the TOA.

The comparison with the literature is not trivial because of the location of Ersa and Palma: clean, insular sites at the crossroads of European and North African air masses; and the limited sun position (50 < SZA < 60º). Concerning the background aerosols, García et al. (2012a) showed that for oceanic and clean sites the annual ARF given for SZA = 60 ± 5º was low (< 10 $W \cdot m^{-2}$) and rather similar at the BOA and TOA ($ARF_{TOA} / ARF_{BOA} > 0.7$). The situation $ARF_{TOA} / ARF_{BOA} > 0.7$ is found at Ersa in autumn and at Palma in winter and spring and may indicate the seasons at each site when background aerosols dominate. It is worth further comparing our results to those of García et al. (2012a; 2012b), in particular from the regions R1 (the northern part of the Sahara-Sahel desert area; mineral dust) and R8 (Europe; urban and industrial pollution) which surround our study area. Interestingly in R8 the largest ARF_{BOA} is reached during winter/spring ($-65 < ARF_{BOA} < -45$ $W \cdot m^{-2}$). The same phenomenon occurs at Ersa but with lower values ($ARF_{BOA} \sim -18$ $W \cdot m^{-2}$). Our findings are usually lower than results from case studies: Derimian et al. (2008) found dust ARF_{BOA} (ARF_{TOA}) at SZA = 50º and $AOD_{440} = 0.54$ on the order of -80 (-25) $W \cdot m^{-2}$ at M'Bour, Senegal; Cachorro et al. (2008) found dust ARF_{BOA} (ARF_{TOA}) at 53 < SZA < 75º and $AOD_{440} \sim 0.5$ on the order of -60 (-30) $W \cdot m^{-2}$ at El Arenosillo, Spain; Lyamani et al. (2006) found ARF_{BOA} (ARF_{TOA}) at SZA = 50º of -43 (-8) $W \cdot m^{-2}$ for dust and -33 (-8) $W \cdot m^{-2}$ for European–Mediterranean air masses at Granada, Spain; Formenti et al. (2002) found for aged biomass burning with $AOD_{500} = 0.39$ an ARF_{BOA} (ARF_{TOA}) relatively constant with SZA on the order of -78 (-26) $W \cdot m^{-2}$ over northeastern Greece. Conversely, at Lampedusa, Italy, under a weak dust intrusion ($AOD_{500} = 0.23$ and SSA = 0.96) Meloni et al. (2005) found an ARF_{BOA} (ARF_{TOA}) at SZA = 50º on the order of -13 (-7) $W \cdot m^{-2}$, lower than the summer means at Ersa and Palma. A few years later at the same site but under a stronger dust intrusion ($AOD_{500} = 0.59$) Meloni et al. (2015) found an ARF_{BOA} (ARF_{TOA}) at SZA = 55º on the order of -63 (-45) $W \cdot m^{-2}$, much larger than the summer means found in our work.

The aerosol radiative forcing efficiency at Ersa shows an annual cycle (Figure 10b), the one at the TOA being reverse of the one at the BOA. Relatively constant minimum absolute values at the BOA [-150; -134 $W \cdot m^{-2}$] are reached during the period April – October while maximum

absolute values at the TOA [-107; -100 W·m^{-2}] are reached during the same period. The ARFE at Palma also shows a clear annual cycle but with some irregularities compared to Ersa. $ARFE_{BOA}$ reaches minimum absolute values from February to October [-133; -117 W·m^{-2}], excepting the month of June, while $ARFE_{TOA}$ has a triangular shape with a maximum in January (-110 W·m^{-2}) and a minimum in June (-71 W·m^{-2}). The reverse behaviour of $ARFE_{BOA}$ (maximum) and $ARFE_{TOA}$ (minimum) in June is due to the combination of 1) the strong increase (in absolute value) of ARF_{BOA} between May and June while ARF_{TOA} increases very little and 2) the strong increase of AOD from May to June (Figure 4a). The annual mean of $ARFE_{TOA}$ is lower at Palma (-85.1 W·m^{-2}, SSA$_{440}$ ~ 0.92) than at Ersa (-99.2 W·m^{-2}, SSA$_{440}$ ~ 0.96) which reflects that more absorbing aerosols produce a lower absolute $ARFE_{TOA}$ (García et al., 2012b).

García et al. (2012b) produced summer mean values of $ARFE_{BOA}$ ($ARFE_{TOA}$) for SZA = 60 ± 5º in regions R1 (dust) and R8 (urban/industrial) of approximately -150 (-50) and -165 (-70) W·m^{-2}, respectively, and winter mean values in R13 (oceanic) of approximately -145 (-100) W·m^{-2}. The annual $ARFE_{BOA}$ at Ersa (-144.4 W·m^{-2}) and at Palma (-132.2 W·m^{-2}) are slightly lower than the values given by García et al. (2012b) but are within the error bars. The explanation is probably that neither Ersa nor Palma are dominated by any of the aforementioned aerosol types but are rather representative of a mixture of them. García et al. (2012b) also showed that the mean $ARFE_{BOA}$ in other dust regions (R2, western Africa) could be lower (-100 W·m^{-2}). The relatively large (in absolute value) annual $ARFE_{TOA}$ at Ersa (-99.2 W·m^{-2}) and at Palma (-85.1 W·m^{-2}) compared to the results of García et al. (2012b) indicate that $ARFE_{TOA}$, like ARF_{TOA}, is not strongly affected by long-range transport aerosols. Other works like Derimian et al. (2008) found dust $ARFE_{BOA}$ ($ARFE_{TOA}$, both w.r.t. AOD$_{440}$) at SZA = 50º on the order of -150 (-45) W·m^{-2} at M'Bour, Senegal. Di Sarra et al. (2008) made a multi-year statistical study at Lampedusa, Italy, and found $ARFE_{BOA}$ (w.r.t. AOD$_{496}$) at 50 < SZA < 60º on the order of -155 W·m^{-2} for dust and -135 W·m^{-2} for biomass burning/industrial aerosols. All studies show that while $ARFE_{BOA}$ for dust is hardly dependent on AOD$_\lambda$, it is highly dependent on AOD$_\lambda$ for biomass burning/industrial aerosols. Likewise, Di Biagio et al. (2009) found also at Lampedusa $ARFE_{BOA}$ (w.r.t. AOD$_{496}$) at 50 < SZA < 60º on the order of -180 W·m^{-2} for dust and -140 W·m^{-2} for urban/industrial aerosols . During a strong dust intrusion at

Lampedusa (AOD_{500} = 0.59) Meloni et al. (2015) found an $ARFE_{BOA}$ ($ARFE_{TOA}$, both w.r.t. AOD_{500}) at SZA = 55º on the order of -107 (-77) $W \cdot m^{-2}$, much lower than both previous works at the same site (Di Sarra et al., 2008; Di Biagio et al., 2009) and than the summer means found in our work. The reason given by Meloni et al. (2015) is that they used higher SSA values than the ones associated to mineral dust at Lampedusa.

In summary the aerosol radiative forcing at 50 < SZA < 60º in the western Mediterranean Basin is usually lower than case studies at sites dominated by only one aerosol type (dust or urban/industrial aerosols). During the spring (at Ersa) and summer (at Palma) months when dust episodes are more frequent an increase of ARF_{BOA} is observed. At the TOA a maximum is reached in summer at both sites (Ersa and Palma have roughly the same ARF_{TOA}). The annual cycle of the aerosol radiative forcing efficiency, which unlike the ARF does not depend on the column aerosol amount, is not as marked as that of the ARF. The explanation comes from the higher dependency of the ARFE to absorption properties which are quite variable over the western Mediterranean Basin, especially for mineral dust.

7 On the possible NE–SW gradients of the aerosol properties during August-December 2011

In this last Section we are also additionally considering the third site at Alborán Island (see map in Figure 1) to examine possible NE–SW gradients of the aerosol properties. Although data at Alborán are available from June 2011 to January 2012, the coincident period with simultaneous measurements at all three sites is limited to August to December 2011. The following analysis is based on data from this 5-month period. In that particular period, very few AERONET level 2.0 inversion products (with the following restrictions: 50 < SZA < 80º and AOD_{440} > 0.4) are available: 3 measurements at Ersa, 7 at Palma and 5 at Alborán. For that reason the AERONET products for which these restrictions apply (AAOD, AAE, RRI, IRI and SSA) are not analyzed in the following. Two products, ARF and ARFE, have too fee measurements available in December and are shown only in the period August to November 2011.

We first plot in Figure 11 the (δAE, AE) plots at the three sites to get an insight into the aerosol types found during the period 08 – 12/2011. The fraction of points with AOD_{675} > 0.15 with respect to the total number of measurements increases from North to South: 7, 11 and 38 % at Ersa, Palma and Alborán, respectively. In all three sites only a small number of cases correspond to a fine mode cluster (η > 70 %; 0.10 < r^f < 0.15 μm). At Ersa most of the points have a fine mode radius between 0.10 and 0.15 μm. One can distinguish easily a cluster formed

most probably by maritime + continental aerosols ($0.75 < AE < 1.3$; $30 < \eta < 70$ %) and another one formed by mineral dust ($\delta AE < 0.3$; $AE < 0.75$). These two aerosol types also appear in the Palma plot. Compared to Ersa, the cluster formed by maritime +continental aerosols at Palma is moved towards ($0.5 < AE < 1.2$; $10 < \eta < 50$ % and $r^f < 0.10$ μm). At Alborán a single large cluster is visible at ($0 < \delta AE < 0.4$; $AE < 1.3$) which indicates that maritime + continental aerosols and mineral dust have a similar signature in the (δAE, AE) representation. This first analysis reveals that the considered period from August to December 2011 seems to have been dominated by rather large particles and an increasing number from North to South of cases with large AODs. It is important to recall that at Alborán 35 % of the days were dominated by maritime +continental aerosols and 31 % by mineral dust during the period June 2011 – January 2012 (Lyamani et al., 2015; Valenzuela et al., 2015; see also Section 4.2).

The same general decreasing tendency of AOD_{440} (Figure 11d) is observed at all three sites from August to December 2011. During the first three months an increasing NE–SW gradient is observed. The NE–SW gradient of the amount of the fine mode particles, shown by AOD^{f}_{440} (Figure 11e), is not that clear. In August and September AOD^{f}_{440} seems to follow a slightly decreasing NE–SW gradient, although all monthly means are within one another standard deviations. Our findings, in agreement with Lyamani et al. (2015), suggest a rather homogeneous spatial distribution of the fine particle loads over the three sites in spite of the distances between the sites and the differences in local sources. $AE_{440\text{-}870}$ (Figure 11f) present a clear decreasing NE–SW gradient during the whole period 08 – 12/2011 which is the signature of an increasing contribution of large particles from North to South. This result is also reflected by the average size distribution shown in Figure 11i where the coarse mode volume concentration has a clear increasing NE–SW gradient. Let's note, en passant, that the fine mode volume concentration is not significantly different at all three sites, which supports the previous hypothesis of a rather homogeneous spatial distribution of the fine particles. The asymmetry factor at 440 nm (Figure 11j) shows an increasing NE–SW gradient with g_{440} values in the range 0.69 – 0.70 at Ersa and Palma and ~0.75 at Alborán. According to Dubovik et al. (2002b) urban/industrial aerosols and desert dust have a similar g_{440} (0.68-0.73) and maritime aerosols have a slightly higher g_{440} (~0.75). Both g spectra at Ersa and Palma are indeed similar to the autumn average (Figure 8b2). We can thus deduce that g is associated to pollution at Ersa (low g and strong spectral dependency), to pollution and mineral dust at Palma (low g and low spectral dependency) and could be attributed to maritime aerosols and mineral dust at Alborán (high g and low spectral dependency). Without further information on the aerosol properties at Alborán, these results cannot be further evaluated. Indeed at least two other types of aerosol

are often found in the southern part of the western Mediterranean Basin: from North African urban/industrial origin (Rodríguez et al., 2011) and/or from ship emissions (Valenzuela et al., 2015). The emissions of both types of aerosols have been quantified in the Bay of Algeciras by Pandolfi et al. (2011).

The aerosol direct radiative forcing (Figure 11g) at the BOA shows an increasing (in absolute value) NE–SW gradient. At the TOA ARF is higher (in absolute value) at Alborán but it is similar at Ersa and Palma. Alborán measurements can be compared to ARF of dust in Granada (140 km N–NW of Alborán) from Valenzuela et al. (2012b) who found annual means of ARF_{BOA} (ARF_{TOA}) at SZA = 55 ± 5º for African desert dust events of approximately -50 (-20) $W \cdot m^{-2}$. The difference at the TOA between Alborán and the other two sites may come from low aerosol absorption properties at Alborán ($AAOD_{440}$ < 0.02, see Sicard et al., 2014) producing an increase of ARF_{TOA} (Boucher and Tanré, 2000). The aerosol radiative forcing efficiency at the BOA has a decreasing (in absolute value) NE–SW gradient which denote that particles with higher absorption properties (like Ersa and Palma) will be more efficient in producing forcing at the surface. At the TOA the ARFE has no marked gradient.

8 Conclusion

AERONET products from the period 2011-2015 are compared in two regional background insular sites in the northern (Corsica) and center (Balearic Islands) part of the western Mediterranean Basin. The Gobbi et al. (2007) graphical method, based on (δAE, AE) plots, has been used to classify the aerosols in clusters with the AERONET AOD inversions (no restrictions) and with the AERONET product inversions (50 < SZA < 80º and AOD_{440} > 0.4). The AOD data put forward three large clusters: a fine mode cluster corresponding to aerosols of polluted and continental origin, a coarse mode cluster corresponding to mineral dust and, in between, a cluster corresponding to maritime aerosols mixed with either one. The restrictions which apply to the level 2.0 inversion products filter drastically the (δAE, AE) plots and leave out only two aerosol types: pollution and mineral dust. Out of the product inversions, the highest percentages of mineral dust outbreaks occur in spring at Ersa (64 %) and in summer at Palma (84 %), while for pollution they occur in summer at both sites (67 and 60 %).

The differences between both sites (Ersa vs. Palma) in the annual mean of aerosol properties like AOD_{440} (0.16 vs. 0.18), $AE_{440–870}$ (1.37 vs. 1.14) and coarse mode volume concentration (0.027 vs. 0.046 $\mu m^3 \cdot \mu m^{-2}$) indicate that in average larger particles are found at Palma (vs. Ersa) which suggests that mineral dust is the main driver of these properties on a yearly basis. AOD_{440}

reaches maxima in summer and minima in winter. Higher AOD_{440} values are observed at Ersa in spring and at Palma in summer and reflect, respectively, a contribution of aerosols of continental origin already in spring over Ersa and not before summer over Palma, and a higher frequency of mineral dust outbreaks at Palma in summer. The fine mode AOD_{440} is similar at both sites all year round except in spring when the presence of aerosols of continental origin already in spring over Ersa contributes to increase AOD^{f}_{440}. This result, reinforced by a yearly fine mode size distribution quasi-identical at both sites, suggests a rather homogeneous spatial distribution of the fine particle loads over both sites in spite of the distances between the sites and the differences in local sources.

The absorption properties were retrieved from AERONET level 2.0 inversion products with the following restrictions 50 < SZA < 80º and AOD_{440} > 0.4 (AAOD, AAE, complex refractive index and SSA) for the two types of aerosols able to produce large AOD values: pollution and mineral dust. The seasonal variability was assessed for both pollution and mineral dust cases separately, and for the total cases (pollution + mineral dust). The two latter aerosols have very different signature in terms of amplitude and spectra of the absorption properties. Their separate analysis (and previous classification) is thus the only way to identify their signature in the total means. Except in summer at Palma where the total and the mineral dust seasonal means are nearly equal (because mineral dust represents 84 % of the total), the absorption properties (magnitude and spectral dependency) of the total present the signature of neither pollution, nor mineral dust, but a mixture of both. The mineral dust cases are associated with higher AAOD and AAE ($0.023 < AAOD_{440} < 0.057$ and $1.43 < AAE < 2.69$) and lower SSA ($0.89 < SSA_{440} < 0.95$) than pollution ($AAOD_{440} < 0.02$, $1.10 < AAE < 1.24$ and $0.97 < SSA_{440} < 0.98$) and present larger inter-season and inter-site variations.

The asymmetry factor, which represents a measure of the preferred scattering direction of special importance for direct radiative forcing estimations, showed very little inter-season and inter-site variations: g_{440} ranged within 0.71 – 0.73 for mineral dust with no spectral dependency and within 0.68 – 0.70 for pollution with a general tendency to decrease with increasing wavelengths. The radiative forcing at the surface filtered for 50 ≤ SZA ≤ 60º reaches its maximum (in absolute value) during spring at Ersa (-18.0 $W \cdot m^{-2}$) and summer at Palma (-22.8 $W \cdot m^{-2}$). In spring ARF_{BOA} is almost double at Ersa w.r.t. Palma, spring being the season at Ersa of the beginning of pollution episodes and of the peak of mineral dust events. ARF_{TOA} reaches summer maxima (in absolute value) of ~ -13.0 $W \cdot m^{-2}$ at both sites. The radiative forcing efficiency annual cycles show some irregularities and have quite different shapes at

both sites. Annual means of $ARFE_{BOA}$ and $ARFE_{TOA}$ are, respectively, -144.4 and -99.2 W·m^{-2} at Ersa and -132.2 and -85.1 W·m^{-2} at Palma which points out that on average the aerosol mixing at Ersa is more efficient in producing forcing than the one at Palma.

A few months, from August to December 2011, of AERONET measurements available in a third site in the southern part of the western Mediterranean Basin (Alborán Island) are considered to examine possible North – South gradients over the whole western Mediterranean Basin. The comparison between the three sites has shown an increasing number of events with large AOD and with larger particles from North to South. As a consequence AOD_{440} and C_V^c increases while $AE_{440\text{-}870}$ decreases from North to South. The fine mode AOD and particle volume size distribution have no marked gradient which again supports one of the findings of this work that confirms a rather homogeneous spatial distribution of the fine particle loads in the western Mediterranean Basin. At the surface the aerosol forcing increases from North to South, while its efficiency decreases. At the TOA no clear gradient is observed for both quantities. It is in partly due to the large variability of the absorption properties, especially for mineral dust, which was previously demonstrated.

In summary, a North-South gradient exist in the western Mediterranean Basin for the aerosol amount (AOD) and especially its coarse mode, which all together produces a similar gradient of the aerosol radiative forcing. The aerosol fine mode is rather homogeneously distributed. Absorption properties are quite variable because of the many and different sources of anthropogenic particles in and around the western Mediterranean Basin: North African and European urban areas, the Iberian and Italian Peninsulas, forest fures and ship emissions. As a result the aerosol forcing efficiency, more dependent to absorption than the forcing, has no marked gradient. The high variations observed on the absorption of mineral dust support the hypothesis of an anthropogenic influence as already formulated by Valenzuela et al. (2015). In the framework of ChArMEx, ongoing investigations might bring some light in the near future to the anthropogenic particle issue and their mixing with the natural particles transported over the western Mediterranean Basin.

Acknowledgements

This study is performed in the framework of work package 4 on aerosol-radiation-climate interactions of the coordinated program ChArMEx (the Chemistry-Aerosol Mediterranean Experiment; http://charmex.lsce.ipsl.fr). It is also supported by the ACTRIS (Aerosols, Clouds, and Trace Gases Research Infrastructure Network) Research Infrastructure Project funded by

the European Union's Horizon 2020 research and innovation programme under grant agreement n. 654169 and previously under grant agreement n. 262254 in the 7th Framework Programme (FP7/2007-2013); by the Spanish Ministry of Economy and Competitivity (project TEC2012-34575) and of Science and Innovation (project UNPC10-4E-442) and EFRD (European Fund for Regional Development); by the Department of Economy and Knowledge of the Catalan autonomous government (grant 2014 SGR 583); and by the Andalusia Regional Government through projects P12-RNM-2409 and P10-RNM-6299. ChArMEx-France is supported through the MISTRALS program by INSU, ADEME, Météo-France, and CEA. The The Spanish Agencia Estatal de Meteorología (AEMET) is acknowledged for the use of the Palma de Mallorca AERONET sun-photometer data, and the Royal Institute and Observatory of the Spanish Navy (ROA) for the support provided at Alborán. The authors want also to thank A. Gkikas for information on intense dust episodes at the 3 AERONET sites.

References

AERONET: AERONET Version 2 Inversion Product Descriptions: http://aeronet.gsfc.nasa.gov/new_web/Documents/Inversion_products_V2.pdf, last access: 11 April 2016.

Albrecht, B. A.: Aerosols, cloud microphysics and fractional cloudiness, Science, 245, 1227–1230, doi:10.1126/science.245.4923.1227, 1989.

Barnaba, F., and Gobbi, G. P.: Aerosol seasonal variability over the Mediterranean region and relative impact of maritime, continental and Saharan dust particles over the basin from MODIS data in the year 2001, Atmos. Chem. Phys., 4, 2367–2391, doi: 10.5194/acp-4-2367-2004, 2004.

Basart, S., Pérez, C., Cuevas, E., Baldasano, J. M., and Gobbi, G. P.: Aerosol characterization in Northern Africa, Northeastern Atlantic, Mediterranean Basin and Middle East from direct-sun AERONET observations, Atmos. Chem. Phys., 9, 8265–8282, doi: 10.5194/acp-9-8265-2009, 2009.

Bergametti, G., Gomes, L., Remoudaki, E., Desbois, M., Martin, D., and Buat-Ménard, P.: Present transport and deposition patterns of African dusts to the north-western Mediterranean, In Paleoclimatology and Paleometeorology: Modern and Past Patterns of Global Atmospheric Transport. Leinen, M., and Sarnthein, M., Eds., Kluwer, 227-251, 1989.

Bergametti, G., Remoudaki, E., Losno, R., Steiner, E., Chatenet, B. and Buat-Mnard, P.: Source, transport and deposition of atmospheric phosphorus over the northwestern Mediterranean, J. Atmos. Chem., 14, 501–513, doi: 10.1007/BF00115254, 1992.

Bergstrom, R.W., Pilewskie, P., Russell, P. B., Redemann, J., Bond, T. C., Quinn, P. K., and Sierau, B.: Spectral absorption properties of atmospheric aerosols, Atmos. Chem. Phys., 7, 5937–5943, doi: 10.5194/acp-7-5937-2007, 2007.

Boucher, O., and Tanré, D.: Estimation of the aerosol perturbation to the Earth's radiative budget over oceans using POLDER satellite aerosol retrievals, Geophys. Res. Lett., 27, 1103– 1106, doi: 10.1029/1999GL010963, 2000.

Cachorro, V. E., Toledano, C., Prats, N., Sorribas, M., Mogo, S., Berjón, A., Torres, B., Rodrigo, R., de la Rosa, J., and De Frutos, A. M.: The strongest desert dust intrusion mixed with smoke over the Iberian Peninsula registered with Sun photometry, J. Geophys. Res., 113, D14S04, doi: 10.1029/2007JD009582, 2008.

CERES: CERES Terra Edition2B SSF TOA Fluxes - Accuracy and Validation: https://eosweb.larc.nasa.gov/sites/default/files/project/ceres/quality_summaries/ssf_toa_terra_ed2B.pdf, last access: 11 April 2016.

Denjean, C., Cassola, F., Mazzino, A., Triquet, S., Chevaillier, S., Grand, N., Bourrianne, T., Momboisse, G., Sellegri, K., Schwarzenbock, A., Freney, E., Mallet, M., and Formenti, P.: Size distribution and optical properties of mineral dust aerosols transported in the western Mediterranean, Atmos. Chem. Phys., 16, 1081-1104, doi: 10.5194/acp-16-1081-2016, 2016.

Derimian, Y., Léon, J.-F., Dubovik, O., Chiapello, I., Tanré, D., Sinyuk, A., Auriol, F., Podvin, T., Brogniez, G., and Holben, B. N.: Radiative properties of aerosol mixture observed during the dry season 2006 over M'Bour, Senegal (African Monsoon Multidisciplinary Analysis campaign), J. Geophys. Res., 113, D00C09, doi: 10.1029/2008JD009904, 2008.

Di Biagio, C., Di Sarra, A., Meloni, D., Monteleone, F., Piacentino, S., and Sferlazzo, D.: Measurements of Mediterranean aerosol radiative forcing and influence of the single scattering albedo, J. Geophys. Res., 114, D06211, doi:10.1029/2008JD011037, 2009.

Di Sarra, A., Pace, G., Meloni, D., De Silvestri, L., Piacentino, S., and Monteleone, F.: Surface shortwave radiative forcing of different aerosol types in the Mediterranean, Geophys. Res. Lett., 35, L02714, doi: 10.1029/2007GL032395, 2008.

Dubovik, O. and King, M. D., A flexible inversion algorithm for retrieval of aerosol optical properties from Sun and sky radiance measurements, J. Geophys. Res., 105, 20673–20696, doi: 10.1029/2000JD900282, 2000a.

Dubovik, O., Smirnov, A., Holben, B.N., King, M.D., Kaufman, Y. J., Eck, T.F., and Slutsker, I.: Accuracy assessment of aerosol optical properties retrieval from AERONET sun and sky radiance measurements, J. Geophys. Res ,105, 9791-9806, doi: 10.1029/2000JD900040, 2000b.

Dubovik, O., Holben, B. N., Lapyonok, T., Sinyuk, A., Mishchenko, M. I., Yang, P., and Slutsker, I.: Non-spherical aerosol retrieval method employing light scattering by spheroids, Geophys. Res. Lett., 10, 1415, doi: 10.1029/2001GL014506, 2002a.

Dubovik, O., Holben, B. N., Eck, T. F., Smirnov, A., Kaufman, Y. J., King, M. D., Tanré, D., and Slutsker, I.: Variability of absorption and optical properties of key aerosol types observed in worldwide locations, J. Atmos. Sci., 59, 590–608, 2002b.

Dubovik, O., Sinyuk, A., Lapyonok, T., Holben, B. N., Mishchenko, M., Yang, P., Eck, T. F., Volten, H., Muñoz, O., Veihelmann, B., van der Zande, W. J., Leon, J.-F., Sorokin, M., and

Slutsker, I.: Application of spheroid models to account for aerosol particle nonsphericity in remote sensing of desert dust, J. Geophys. Res., 111, D11208, doi:10.1029/2005JD006619, 2006.

Dubuisson, P., Buriez, J.C., and Fouquart, Y.: High spectral resolution solar radiative transfer in absorbing and scattering media: Application to the satellite simulation, J. Quant. Spectros. Radiat. Transfer., 55, 103-126, doi: 10.1016/0022-4073(95)00134-4, 1996.

Dubuisson, P., Dessailly, D., Vesperini, M., and Frouin, R.: Water Vapor Retrieval Over Ocean Using Near-Infrared Radiometry, J. Geophys. Res., 109, D19106, doi:10.1029/2004JD004516, 2004.

Dubuisson, P., Roger, J., Mallet, M., and Dubovik, O.: A Code to Compute the Direct Solar Radiative Forcing: Application to Anthropogenic Aerosols during the Escompte Experiment, Proc. International Radiation Symposium (IRS 2004) on Current Problems in Atmospheric Radiation, edited by: Fischer, H., Sohn, B.-J., and Deepak, A., Hampton, 127–130, 23–28 August 2004, Busan, Korea, 2006.

Dulac, F., An overview of the Chemistry-Aerosol Mediterranean Experiment (ChArMEx), European Geosciences Union General Assembly, Geophys Res. Abstracts, 16, EGU2014-11441, Vienna (Austria), 27 April – 2 May 2014.

Eck, T. F., Holben, B. N., Reid, J. S., Dubovik, O. Kinne, S., Smirnov, A., O'Neill, N. T., and Slutsker, I.: Wavelength dependence of the optical depth of biomass burning, urban and desert dust aerosols, J. Geophys. Res., 104, 31333-31349, doi: 10.1029/1999JD900923, 1999.

Escudero, M., Querol, X., Ávila, A., and Cuevas, E.: Origin of the exceedances of the European daily PM limit value in regional background areas of Spain, Atmos. Environ., 41, 730–744, doi: 10.1016/j.atmosenv.2006.09.014, 2007.

Formenti, P., Boucher, O. Reiner, T., Sprung, D., Andreae, M. O., Wendisch, M., Wex, H., Kindred, D., Tzortziou, M., Vasaras, A., and Zerefos, C.: STAAARTE-MED 1998 summer airborne measurements over the Aegean Sea: 2. Aerosol scattering and absorption, and radiative calculations, J. Geophys. Res., 107(D21), 4551, doi:10.1029/2001JD001536, 2002.

Gangoiti, G., Millán, M. M., Salvador, R., and Mantilla, E.: Long-range transport and re-circulation of pollutants in the western Mediterranean during the project Regional Cycles of Air Pollution in the West-Central Mediterranean Area, Atmos. Environ., 35, 6267-6276, doi: 10.1016/S1352-2310(01)00440-X, 2001.

García, O. E., Díaz, A. M., Expósito, F. J., Díaz, J. P., Dubovik, O., Dubuisson, P., Roger, J.-C., Eck, T. F., Sinyuk, A., Derimian, Y., Dutton, E. G., Schafer, J. S., Holben, B. N., and García, C. A., Validation of AERONET estimates of atmospheric solar fluxes and aerosol radiative forcing by ground-based broadband measurements, J. Geophys. Res., 113, D21207, doi:10.1029/2008JD010211, 2008.

García, O. E., Expósito, F. J., Díaz, J. P., and Díaz, A. M.: Radiative forcing under aerosol mixed conditions, J. Geophys. Res., 116, D01201, doi:10.1029/2009JD013625, 2011.

García, O.E., Díaz, J.P., Expósito, F.J., Díaz, A.M., Dubovik, O., and Derimian, Y., Aerosol Radiative Forcing: AERONET-Based Estimates, Climate Models, Dr. Leonard Druyan (Ed.), ISBN: 978-953-51-0135-2, InTech, Available from: http://www.intechopen.com/books/climate-models/aerosol-radiative-forcing-aeronet-based-estimates (last access: 16 December 2015), 2012a.

García, O. E., Díaz, J. P., Expósito, F. J., Díaz, A. M., Dubovik, O., Derimian, Y., Dubuisson, P., and Roger, J.-C.: Shortwave radiative forcing and efficiency of key aerosol types using AERONET data, Atmos. Chem. Phys., 12, 5129–5145, doi:10.5194/acp-12-5129-2012, 2012b.

Giorgi, F.: Climate change hot-spots, Geophys. Res. Lett., 33, L08707, doi:10.1029/2006GL025734, 2006.

Giorgi, F. and Lionello, P., Climate change projections for the Mediterranean region, Global Planet. Change, 63, 90–104, doi: 10.1016/j.gloplacha.2007.09.005, 2008.

Gkikas, A., Houssos, E.E., Hatzianastassiou, N., Papadimas, C.D., and Bartzokas, A.: Synoptic conditions favouring the occurrence of aerosol episodes over the broader Mediterranean basin, Q. J. R. Meteorol. Soc., 138, 932–949, doi:10.1002/qj.978, 2012.

Gkikas, A., Basart, S., Hatzianastassiou, N., Marinou, E., Amiridis, V., Kazadzis, S., Pey, J., Querol, X., Jorba, O., Gassó, S., and Baldasano, J. M.: Mediterranean desert dust outbreaks and their vertical structure based on remote sensing data, Atmos., Chem. Phys., 16, in press, 2016.

Gobbi, G. P., Kaufman, Y. J., Koren, I., and Eck, T. F.: Clasification of aerosol properties derived from AERONET direct sun data, Atmos. Chem. Phys. 7, 453–458, doi: 10.5194/acp-7-453-2007, 2007.

Granados-Muñoz, M. J., Navas-Guzmán, F., Bravo-Aranda, J. A., Guerrero-Rascado, J. L., Lyamani, H., Valenzuela, A., Titos, G., Fernández-Gálvez, J., and Alados-Arboledas, L.:

Hygroscopic growth of atmospheric aerosol particles based on active remote sensing and radiosounding measurements: selected cases in southeastern Spain, Atmos. Meas. Tech., 8, 705-718, doi:10.5194/amt-8-705-2015, 2015.

Guieu, C., Bonnet, S., and Wagener, T.: Biomass burning as a source of dissolved iron to the open ocean?, Geophys. Res. Lett., 32, L19608, doi:10.1029/2005GL022962, 2005.

Holben, B. N., Eck, T. F., Slutsker, I., Tanré, D., Buis, J. P., Setzer, A., Vermote, E. F., Reagan, J. A., Kaufman, Y. J., Nakajima, T., Lavenu, F., Jankowiak, I., and Smirnov, A., AERONET – A federated instrument network and data archive for aerosol characterization, Remote Sens. Environ., 66, 1–16, doi:10.1016/S0034-4257(98)00031-5, 1998.

Holben, B.N., Eck, T. F., Slutsker, I., Smirnov, A., Sinyuk, A., Schafer, J., Giles, D., and Dubovik, O.: AERONET's Version 2.0 quality assurance criteria, in Remote Sensing of the Atmosphere and Clouds, edited by: Tsay, S.-C., Nakajima, T., Ramesh P. S., and Sridharan, R., Proc. of SPIE Vol. 6408, 64080Q, doi: 10.1117/12.706524, 2006.

Hurrell, J. W.: Decadal trends in the North Atlantic Oscillation: Regional temperatures and precipitation, Science, 269, 676-679, doi: 10.1126/science.269.5224.676, 1995.

Kallos, G., Astitha, M., Katsafados, P., and Spyrou, C.: Long-range transport of anthropogenically and naturally produced particulatematter in the Mediterranean and North Atlantic: Current state of knowledge, J. Appl. Meteorol. Clim., 46, 1230–1251, doi: 10.1175/JAM2530.1, 2007.

Kaufman, Y. J.: Aerosol optical thickness and atmospheric path radiance, J. Geophys. Res., 98, 2677–2692, doi: 10.1029/92JD02427, 1993.

Lack, D. A. and Cappa, C. D.: Impact of brown and clear carbon on light absorption enhancement, single scatter albedo and absorption wavelength dependence of black carbon, Atmos. Chem. Phys., 10, 4207–4220, doi:10.5194/acp-10-4207-2010, 2010.

Lambert, D. and Argence, S.: Preliminary study of an intense rainfall episode in Corsica, 14 September 2006, Adv. Geosci., 16, 125-129, 2008.

Lambert, D., Mallet, M., Ducrocq, V., Dulac, F., Gheusi, F., and Kalthoff, N.: CORSiCA: a Mediterranean atmospheric and oceanographic observatory in Corsica within the framework of HyMeX and ChArMEx, Adv. Geosci., 26, 125-131, doi:10.5194/adgeo-26-125-2011, 2011.

Lelieveld, J., Berresheim, H., Borrmann, S., Crutzen, P.J., Dentener, F.J., Fischer, H., Feichter, J., Flatau, P.J., Heland, J., Holzinger, R., Korrmann, R., Lawrence, M.G., Levin, Z.,

Markowicz, K.M., Mihalopoulos, N., Minikin, A., Ramanathan, V., de Reus, M., Roelofs, G.J., Scheeren, H.A., Sciare, J., Schlager, H., Schultz, M., Siegmund, P., Steil, B., Stephanou, E.G., Stier, P., Traub, M.,Warneke, C., Williams, J., and Ziereis, H.: Global air pollution crossroads over the Mediterranean, Science, 298, 794–799, doi: 10.1126/science.1075457, 2002.

Loeb, N. G., Kato, S., Loukachine, K., Manalo-Smith, N., and Doelling, D. R.: Angular Distribution Models for Top-of-Atmosphere Radiative Flux Estimation from the Clouds and the Earth's Radiant Energy System Instrument on the Terra Satellite. Part II: Validation, J. Atmos. Oceanic Technol., 24, 564-584, doi:10.1175/JTECH1983.1, 2007.

Lyamani, H., Olmo, F. J., Alcántara, A., and Alados-Arboledas, L.: Atmospheric aerosols during the 2003 heat wave in southeastern Spain II: Microphysical columnar properties and radiative forcing, Atmos. Environ., 40, 6465–6476, doi: 10.1016/j.atmosenv.2006.04.047, 2006.

Lyamani, H., Fernández-Gálvez, J., Pérez-Ramírez, D., Valenzuela, A., Antón, M., Alados, I., Titos, G., Olmo, F.J., Alados-Arboledas, L.: Aerosol properties over two urban sites in South Spain during an extended stagnation episode in winter season, Atmos. Environ., 62, 424-432, http://dx.doi.org/10.1016/j.atmosenv.2012.08.050 2012.

Lyamani, H., Valenzuela, A., Perez-Ramirez, D., Toledano, C., Granados-Muñoz, M. J., Olmo, F. J., and Alados-Arboledas, L.: Aerosol properties over the western Mediterranean basin: temporal and spatial variability, Atmos. Chem. Phys., 15, 2473-2486, doi: 10.5194/acp-15-2473-2015, 2015.

Maheras, P., Xoplaki, E., Davies, T., Vide, J. V., Bariendos, M., and Alcoforado, M.: Warm and cold monthly anomalies across the Mediterranean basin and their relationship with circulation: 1860–1990, Int. J. Climatol., 19, 1697-1715, doi: 10.1002/(SICI)1097-0088(199912)19:15<1697::AID-JOC442>3.0.CO;2-S, 1999.

Mallet, M., Dubovik, O., Nabat, P., Dulac, F., Kahn, R., Sciare, J., Paronis, D. and Léon, J. F., Absorption properties of Mediterranean aerosols obtained from multi-year ground-based remote sensing observations, Atmos. Chem. Phys., 13, 9195–9210, doi:10.5194/acp-13-9195-2013, 2013.

Mallet, M., Dulac, F., Formenti, P., Nabat, P., Sciare, J., Roberts, G., Pelon, J., Ancellet, G., Tanré, D., Parol, F., di Sarra, A., Alados, L., Arndt, J., Auriol, F., Blarel, L., Bourrianne, T., Brogniez, G., Chazette, P., Chevaillier, S., Claeys, M., D'Anna, B., Denjean, C., Derimian,

Y., Desboeufs, K., Di Iorio, T., Doussin, J.-F., Durand, P., Féron, A., Freney, E., Gaimoz, C., Goloub, P., Gómez-Amo, J. L., Granados-Muñoz, M. J., Grand, N., Hamonou, E., Jankowiak, I., Jeannot, M., Léon, J.-F., Maillé, M., Mailler, S., Meloni, D., Menut, L., Momboisse, G., Nicolas, J., Podvin, J., Pont, V., Rea, G., Renard, J.-B., Roblou, L., Schepanski, K., Schwarzenboeck, A., Sellegri, K., Sicard, M., Solmon, F., Somot, S., Torres, B., Totems, J., Triquet, S., Verdier, N., Verwaerde, C., Wenger, J., and Zapf, P.: Overview of the Chemistry-Aerosol Mediterranean Experiment/Aerosol Direct Radiative Forcing on the Mediterranean Climate (ChArMEx/ADRIMED) summer 2013 campaign, Atmos. Chem. Phys., 16, 455–504, doi: 10.5194/acp-16-455-2016, 2016.

Mariotti, A., Pan, Y., Zeng, N., and Alessandri, A.: Long-term climate change in the Mediterranean region in the midst of decadal variability, Clim. Dynam., 44, 1437–1456, doi: 10.1007/s00382-015-2487-3, 2015.

Markowicz, K. M., Flatau, P. J., Ramana, M. V., Crutzen, P. J., and Ramanathan, V., Absorbing Mediterranean aerosols lead to a large reduction in the solar radiation at the surface, Geophys. Res. Lett., 29, 1968, doi:10.1029/2002GL015767, 2002.

Meloni, D., di Sarra, A., Di Iorio, T., and Fiocco G.: Influence of the vertical profile of Saharan dust on the visible direct radiative forcing, J. Quant. Spectrosc. Radiat. Transfer, 93, 397–413, doi: 10.1016/j.jqsrt.2004.08.035, 2005.

Meloni, D., Junkermann, W., di Sarra, A., Cacciani, M., De Silvestri, L., Di Iorio, T., Estellés, V., Gómez-Amo, J. L., Pace, G., and Sferlazzo, D. M.: Altitude-resolved shortwave and longwave radiative effects of desert dust in the Mediterranean during the GAMARF campaign: Indications of a net daily cooling in the dust layer, J. Geophys. Res., 120, 3386–3407, doi:10.1002/2014JD022312, 2015.

Millán, M. M., Salvador R., Mantilla E., and Kallos, G.: Photooxidant dynamics in the Mediterranean basin in summer: results from European research projects, J. Geophys. Res., 102, 8811-8823, doi: 10.1029/96JD03610, 1997.

Mishra, A. K., Klingmueller, K., Fredj, E., Lelieveld, J., Rudich, Y., and Koren, I.: Radiative signature of absorbing aerosol over the eastern Mediterranean basin, Atmos. Chem. Phys., 14, 7213-7231, doi:10.5194/acp-14-7213-201, 2014.

Moosmüller, H., Chakrabarty, R. K., and Arnott,W. P., Aerosol light absorption and its measurement: A review, J. Quant. Spectrosc. Radiat. Transf., 110, 844–878, doi: 10.1016/j.jqsrt.2009.02.035, 2009.

Moulin C., Lambert, C. E., Dulac, F., and Dayan, U: Control of atmospheric export of dust from North Africa by the North Atlantic Oscillation, Nature, 387, 691–694, doi: 10.1038/42679, 1997.

Moulin C., Lambert, C. E., Dayan, U., Masson, V., Ramonet, M., Bousquet, P., Legrand, M., Balkanski, Y. J., Guelle, W., Marticorena, B., Bergametti, G., and Dulac, F., Satellite climatology of African dust transport in the Mediterranean atmosphere, J. Geophys. Res., 103, 13137–13144, doi: 10.1029/98JD00171, 1998.

Nabat, P., Solmon, F., Mallet, M., Kok, J. F., and Somot, S.: Dust emission size distribution impact on aerosol budget and radiative forcing over the Mediterranean region: a regional climate model approach, Atmos. Chem. Phys., 12, 10545–10567, doi:10.5194/acp-12-10545-2012, 2012.

Nabat, P., Somot, S., Mallet, M., Chiapello, I., Morcrette, J. J., Solmon, F., Szopa, S., Dulac, F., Collins, W., Ghan, S., Horowitz, L. W., Lamarque, J. F., Lee, Y. H., Naik, V., Nagashima, T., Shindell, D., and Skeie, R.: A 4-D climatology (1979–2009) of the monthly tropospheric aerosol optical depth distribution over the Mediterranean region from a comparative evaluation and blending of remote sensing and model products, Atmos. Meas. Tech., 6, 1287–1314, doi:10.5194/amt-6-1287-2013, 2013.

Nabat, P., Somot, S., Mallet, M., Sanchez-Lorenzo, A., and Wild, M.: Contribution of anthropogenic sulfate aerosols to the changing Euro-Mediterranean climate since 1980, Geophys. Res. Lett., 41, 5605-5611, doi:10.1002/2014GL060798, 2014.

Nabat, P., Somot, S., Mallet, M., Sevault, F., Chiacchio, M., and Wild, M.: Direct and semi-direct aerosol radiative effect on the Mediterranean climate variability using a coupled regional climate system model, Clim. Dyn., 44, 1127-1155, doi:10.1007/s00382-014-2205-6, 2015.

Nicolas, J., Sciare, J., Petit, J.-E., Bonnaire, N., Féron, A., Dulac, F., Hamonou, E., Gros, V., Mallet, M., Lambert, D., Sauvage, S., Léonardis, T., Tison, E., Colomb, A., Fresney., E., Pichon, J.-M., Bouvier, L., Bourrianne, T., and Roberts, G.: New insights on aerosol sources and properties of organics in the west Mediterranean basin, Geophys. Res. Abstracts, 15, EGU2013-12852, Vienna (Austria), 7-12 April 2013.

Norris, J. R., and Wild, M.: Trends in aerosol radiative effects over Europe inferred from observed cloud cover, solar ‘‘dimming’’ and solar ‘‘brightening,’’, J. Geophys. Res., 112, D08214, doi:10.1029/2006JD007794, 2007.

Omar, A.H., Won, J.G., Winker, D.M., Yoon, S.C., Dubovik, O., and McCormick, M.P.: Development of global aerosol models using cluster analysis of Aerosol Robotic Network (AERONET) measurements. J. Geophys. Res., 110, D10S14, doi:10.1029/2004JD004874, 2005.

O'Neill, N. T., Dubovik, O., and Eck, T. F.: Modified Ångström coefficient for the characterization of submicrometer aerosols, App. Opt., 40, 2368-2375, doi: 10.1364/AO.40.002368, 2001.

O'Neill, N. T., Eck, T. F., Smirnov, A., Holben, B. N., and Thulasiraman, S.: Spectral discrimination of coarse and fine mode optical depth, J. Geophys. Res., 108 (D17), 4559-4573, doi: 10.1029/2002JD002975, 2003.

Pace, G., Meloni, D., and di Sarra, A.: Forest fire aerosol over the Mediterranean basin during summer 2003, J. Geophys. Res., 110, D21202, doi: 10.1029/2005JD005986, 2005.

Pandolfi, M., Gonzalez-Castanedo, Y., Alastuey, A., de la Rosa, J. D., Mantilla, E., Sanchez de la Campa, A., Querol, X., Pey, J., Amato, F., and Moreno, T.: Source apportionment of PM_{10} and $PM_{2.5}$ at multiple sites in the strait of Gibraltar by PMF: impact of shipping emissions, Environ. Sci. Pollut. Res., 18, 260–269, doi: 10.1007/s11356-010-0373-4, 2011.

Papadimas, C. D., Hatzianastassiou, N., Mihalopoulos, N., Querol, X., and Vardavas, I.: Spatial and temporal variability in aerosol properties over the Mediterranean basin based on 6-year (2000–2006) MODIS data, J. Geophys. Res., 113, D11205, doi: 10.1029/2007JD009189, 2008.

Pérez, C., Sicard, M., Jorba, O., Comerón, A., and Baldasano, J. M.: Summertime Re-Circulations of Air Pollutants Over the North-Eastern Iberian Coast Observed From Systematic EARLINET Lidar Measurements in Barcelona, Atmos. Environ., 38, 3983-4000, doi: 10.1016/j.atmosenv.2004.04.010, 2004.

Perrone, M. R., De Tomasi, F., and Gobbi, G. P.: Vertically resolved aerosol properties by multi-wavelength lidar measurements, Atmos. Chem. Phys., 14, 1185-1204, doi:10.5194/acp-14-1185-2014, 2014.

Petzold, A., Rasp, K., Weinzierl, B., Esselborn, M., Hamburger, T., Dörnbrack, A., Kandler, K., Schütz, L., Knippertz, P., Fiebig, M., and Virkkula, A.: Saharan dust absorption and refractive index from aircraft-based observations during SAMUM 2006, Tellus, 61B, 118–130, doi:10.1111/j.1600-0889.2008.00383.x, 2009.

Pey, F., Querol, X., and Alastuey, A., Variations of levels and composition of PM10 and PM2.5 at an insular site in the Western Mediterranean, Atmos. Res., 94, 285–299, 2009.

Pey, J., Querol, X., Alastuey, A., Forastiere, F., and Stafoggia, M.: African dust outbreaks over the Mediterranean Basin during 2001–2011: PM10 concentrations, phenomenology and trends, and its relation with synoptic and mesoscale meteorology, Atmos. Chem. Phys., 13, 1395–1410, doi:10.5194/acp-13-1395-2013, 2013.

Pincus, R., and Baker, M. B.:Precipitation, solar absorption, and albedo susceptibility in marine boundary layer clouds, Nature, 372, 250–252, doi:10.1038/372250a0, 1994.

Pruppacher, H. R., and Klett, J. D.: Microphysics of Clouds and Precipitation, Kluwer Academic Publishers, Dordrecht, 1997.

Redemann, J., Turco, R.P., Liou, K.N., Russell, P.B., Bergstrom, R.W., Schmid, B., Livingston, J.M., Hobbs, P.V., Hartley, W.S., Ismail, S., Ferrare, R.A., and Browell, E.V.: Retrieving the vertical structure of the effective aerosol complex index of refraction from a combination of aerosol in situ and remote sensing measurements during TARFOX, J. Geophys. Res., 105, 9949–9970, doi: 10.1029/1999JD901044, 2000.

Ricchiazzi, P., Yang, S., Gautier, C., and Sowle, D.: SBDART: A research and teaching software tool for plane-parallel radiative transfer in the Earth's atmosphere, Bull. Am. Meteorol. Soc., 79, 2101–2114, 1998.

Rodríguez, S., Alastuey, A., Alonso-Perez, S., Querol, X., Cuevas, E., Abreu-Afonso, J., Viana, M., Pérez, N., Pandolfi, M., and de la Rosa, J.: Transport of desert dust mixed with North African industrial pollutants in the subtropical Saharan Air Layer, Atmos. Chem. Phys., 11, 6663–6685, doi: 10.5194/acp-11-6663-2011, 2011.

Russell, P. B., Bergstrom, R. W., Shinozuka, Y., Clarke, A. D., De-Carlo, P. F., Jimenez, J. L., Livingston, J. M., Redemann, J., Dubovik, O., and Strawa, A.: Absorption Angstrom Exponent in AERONET and related data as an indicator of aerosol composition, Atmos. Chem. Phys., 10, 1155–1169, doi:10.5194/acp-10-1155-2010, 2010.

Sanchez-Gomez, E., Somot, S., and Mariotti, A.: Future changes in the Mediterranean water budget projected by an ensemble of regional climate models, Geophys. Res. Lett., 36, L21401, doi:10.1029/2009GL040120, 2009.

Schuster, G. L., Dubovik, O., and Holben, B. N.: Angstrom exponent and bimodal aerosol size distributions, J. Geophys. Res., 111, D07207, doi:10.1029/2005JD006328, 2006.

Sciare, J., Dulac, F., Feron, A., Crenn, V., Sarda Esteve, R., Baisnee, D., Bonnaire, N., Hamonou, E., Mallet, M., Lambert, D., Nicolas, J. B., Bourrianne, T., Petit, J.E., Favez, O., Canonaco, F., Prevot, A., Mocnik, G., Drinovec, L., Marpillat, A., and Serrie, W., Carbonaceous aerosols in the Western Mediterranean during summertime and their contribution to the aerosol optical properties at ground level: First results of the ChArMEx-ADRIMED 2013 intensive campaign in Corsica, European Geosciences Union General Assembly, Geophys. Res. Abstracts, 16, EGU2014-2358, Vienna (Austria), 27 April-2 May 2014.

Sicard, M., Pérez, C., Rocadenbosch, F., Baldasano, J. M., and García-Vizcaino, D.: Mixed-layer depth determination in the Barcelona coastal area from regular lidar measurements: methods, results and limitations, Bound.-Lay. Meteorol., 119, 135-157, doi: 10.1007/s10546-005-9005-9, 2006.

Sicard, M., Totems, J., Barragan, R., Dulac, F., Mallet, M., Comerón, A., Alados-Arboledas, L., Augustin, P., Chazette, P., Léon, J.-F., Olmo, F. J., Renard, J.-B., Rocadenbosch, F.: Variability of Mediterranean aerosols properties at three regional background sites in the western Mediterranean Basin, in Proc. SPIE 9242, Comerón, A., Kassianov, E.I., Schäfer, K., Picard, R.H., Stein, K.,and Gonglewski, J.D., Eds., SPIE, Washington (EE.UU.), (2014), CCC code: 0277-786X/14/$18, doi:10.1117/12.2068694, 2014.

Sinyuk, A., Dubovik, O., Holben, B.N., Eck, T. F., Breon, F.-M., Martonchik, J., Kahn, R., Diner, D. J., Vermote, E. F., Roger, J.-C., Lapyonok, T., and Slutsker, I.: Simultaneous retrieval of aerosol and surface properties from a combination of AERONET and satellite data, Remote Sens. of Environ., 107, 90-108, doi:10.1016/j.rse.2006.07.022, 2007.

Smirnov, A., Holben, B. N., Eck, T. F., Dubovik, O., and Slutsker, I., Clouds creening and quality control algorithms for the AERONET database, Remote Sens. Environ., 73, 337–349, doi: 10.1016/S0034-4257(00)00109-7, 2000.

Smirnov, A., Holben, B. N., Kaufman, Y. J., Dubovik, O., Eck, T. F., Slutsker, I., Pietras, C., and Halthore, R. N., Optical properties of atmospheric aerosol in maritime environments. J. Atmos. Sci., 59, 501–523, doi: 10.1175/1520-0469(2002)059<0501:OPOAAI>2.0.CO;2, 2002.

Stamnes, K., Tsay, S., Wiscombe, W., and Jayaweera, K.: Numerically stable algorithm for discrete–ordinate-method radiative transfer in multiple scattering and emitting layered media, Appl. Optics, 27, 2502–2509, 1988.

Tegen, I., and Lacis, A. A.: Modeling of particle size distribution and its influence on the radiative properties of mineral dust aerosol, J. Geophys. Res., 101, 19237-19244, doi:10.1029/95JD03610, 1996.

Titos, G., Lyamani, H., Cazorla, A., Sorribas, M., Foyo-Moreno, I., Wiedensohler, A. and Alados-Arboledas, L.: Study of the relative humidity dependence of aerosol light-scattering in southern Spain, Tellus B, 66, 24536, http://dx.doi.org/10.3402/tellusb.v66.24536, 2014.

Toledano, C., Cachorro, V. E., Berjon, A., de Frutos, A. M., Sorribas, M., de la Morena, B. A., and Goloub, P.: Aerosol optical depth and Ångström exponent climatology at El Arenosillo AERONET site (Huelva, Spain), Q. J. R. Meteorol. Soc., 133, 795–807, doi: 10.1002/qj.54, 2007.

Twomey, S.: Pollution and the planetary albedo, Atmos. Environ., 8, 1251– 1256, doi:10.1016/0004-6981(74)90004-3, 1974.

Valenzuela, A., Olmo, F.J., Lyamani, H., Antón, M., Quirantes, A., and Alados-Arboledas, L.: Classification of aerosol radiative properties during African desert dust intrusions over southeastern Spain by sector origins and cluster analysis, J. Geophys. Res., 117, D06214, doi:10.1029/2011JD016885, 2012a.

Valenzuela, A., Olmo, F. J., Lyamani, H., Antón, M., Quirantes, A., and Alados-Arboledas, L.: Aerosol radiative forcing during African desert dust intrusions (2005–2010) over Southeastern Spain, Atmos. Chem. Phys., 12, 10331–10351, doi: 10.5194/acp-12-10331-2012, 2012b.

Valenzuela, A., Olmo, F.J., Lyamani, H., Granados-Muñoz, M.J., Antón, M., Guerrero-Rascado, J.L., Quirantes, A., Toledano, C., Pérez-Ramírez, D., and Alados-Arboledas, L., Aerosol transport over the western Mediterranean basin: Evidence of the contribution of fine particles to desert dust plumes over Alborán Island, J. Geophys. Res. Atmos., 119, 14028-14044, doi: 10.1002/2014JD022044, 2015.

		Summer	Autumn	Winter	Spring	Year
				(N) Mean ± Std		
AOD_{440}	Ersa	(17003) 0.19±0.10	(7993) 0.13±0.09	(3692) 0.08±0.05	(7837) 0.16±0.10	(36525) 0.16±0.10
	Palma	(8667) 0.23±0.12	(6062) 0.16±0.11	(1831) 0.07±0.04	(2319) 0.10±0.06	(18879) 0.18±0.12
$AE_{440\text{-}870}$	Ersa	(17003) 1.46±0.45	(7993) 1.40±0.51	(3692) 1.13±0.46	(7837) 1.27±0.44	(36525) 1.37±0.47
	Palma	(8667) 1.14±0.47	(6062) 1.21±0.48	(1831) 1.11±0.43	(2319) 0.99±0.34	(18879) 1.14±0.46
δAE	Ersa	(2809) 0.05±0.22	(633) 0.04±0.25	(24) -0.01±0.17	(843) 0.04±0.23	(4309) 0.05±0.23
	Palma	(2917) 0.29±0.19	(876) 0.13±0.23	(4) 0.05±0.10	(68) 0.34±0.12	(3865) 0.25±0.21
r_V^f	Ersa	(993) 0.16±0.02	(538) 0.17±0.02	(158) 0.18±0.03	(518) 0.17±0.02	(2207) 0.17±0.02
[μm]	Palma	(809) 0.14±0.02	(548) 0.15±0.02	(177) 0.15±0.02	(184) 0.15±0.02	(1718) 0.15±0.02
C_V^f	Ersa	(993) 0.019±0.012	(538) 0.014±0.011	(158) 0.009±0.006	(518) 0.019±0.013	(2207) 0.017±0.012
[$\mu m^3 \cdot \mu m^{-2}$]	Palma	(809) 0.025±0.013	(548) 0.021±0.017	(177) 0.010±0.007	(184) 0.011±0.008	(1718) 0.021±0.014
r_V^c	Ersa	(993) 2.49±0.41	(538) 2.73±0.43	(158) 2.73±0.44	(518) 2.27±0.46	(2207) 2.52±0.46
[μm]	Palma	(809) 2.43±0.41	(548) 2.61±0.37	(177) 2.43±0.37	(184) 2.10±0.44	(1718) 2.46±0.42
C_V^c	Ersa	(993) 0.032±0.036	(538) 0.021±0.040	(158) 0.018±0.021	(518) 0.027±0.053	(2207) 0.027±0.041
[$\mu m^3 \cdot \mu m^{-2}$]	Palma	(809) 0.063±0.063	(548) 0.038±0.052	(177) 0.013±0.011	(184) 0.025±0.021	(1718) 0.046±0.056
$AAOD_{440}$	Ersa	(26) 0.018±0.011	(12) 0.023±0.017	(0) -	(11) 0.035±0.027	(49) 0.023±0.018
	Palma	(57) 0.043±0.019	(25) 0.034±0.021	(0) -	(0) -	(82) 0.040±0.020
$AAE_{440\text{-}870}$	Ersa	(26) 1.64±0.52	(12) 1.28±0.44	(0) -	(11) 2.11±0.89	(49) 1.66±0.66
	Palma	(57) 1.98±0.49	(25) 1.64±0.55	(0) -	(0) -	(82) 1.88±0.53
RRI_{440}	Ersa	(26) 1.45±0.03	(12) 1.46±0.06	(0) -	(11) 1.44±0.04	(49) 1.45±0.04
	Palma	(57) 1.43±0.05	(25) 1.42±0.06	(0) -	(0) -	(82) 1.43±0.06
IRI_{440} ($\times 10^{-3}$)	Ersa	(26) 2.6±1.3	(12) 3.6±1.8	(0) -	(11) 3.6±1.3	(49) 3.1±1.3
	Palma	(57) 4.7±1.6	(25) 4.8±2.3	(0) -	(0) -	(82) 4.7±1.8

Table 1. Summary of the seasonal variations of the following aerosol properties: AOD_{440}, $AE_{440\text{-}870}$, δAE (=$AE_{440\text{-}675}$ – $AE_{675\text{-}870}$), the particle volume size distribution, $AAOD_{440}$, $AAE_{440\text{-}870}$ and the real (RRI) and imaginary (IRI) part of the refractive index at Ersa and Palma derived from AERONET level 2.0 inversion products available in the period 2011 – 2015. r_V and C_V are the volume median radius and the volume concentration, respectively. *f/c* indicate fine and coarse modes, respectively.The values of δAE are given for $AOD_{675} > 0.15$ as suggested by Gobbi et al. (2007). The values of $AAOD_{440}$, $AAE_{440\text{-}870}$, RRI_{440} and IRI_{440} are given for $50 < SZA < 80º$ and $AOD_{440} > 0.40$.

		Summer	Autumn	Winter	Spring	Year
			N (percentage)			
Mineral dust	Ersa	15 (58 %)	4 (33 %)	-	7 (64 %)	26 (53 %)
(δAE < 0.3, AE < 0.75)	Palma	48 (84 %)	10 (40 %)	-	-	58 (71 %)
Pollution	Ersa	11 (42 %)	8 (67 %)	-	4 (36 %)	23 (47 %)
(AE > 1)	Palma	9 (16 %)	15 (60 %)	-	-	24 (29 %)
			AOD_{440} ± Std			
Mineral dust	Ersa	0.50±0.04	0.66±0.31	-	0.61±0.07	0.55±0.17
(δAE < 0.3, AE < 0.75)	Palma	0.51±0.14	0.51±0.09	-	-	0.51±0.13
Pollution	Ersa	0.47±0.07	0.47±0.02	-	0.43±0.03	0.46±0.05
(AE > 1)	Palma	0.46±0.05	0.48±0.04	-	-	0.47±0.04

Table 2. Seasonal number (and percentage of data in parenthesis) and AOD_{440} (± standard deviation) of the (δAE, AE) points fulfilling (δAE < 0.3, AE < 0.75) and corresponding to mineral dust outbreaks, and fulfilling (AE > 1) and corresponding to pollution events. The data are those of Figure 6 (AERONET level 2.0 inversion products available in the period 2011 – 2015, which means that the following criteria apply on these data: 50 < SZA < 80º and AOD_{440} > 0.4).

		Summer	Autumn	Winter	Spring	Year
				(N) Mean±std		
SSA_{440}	Ersa	(26) 0.96±0.02	(12) 0.96±0.02	(0) -	(11) 0.94±0.02	(49) 0.96±0.03
	Palma	(57) 0.92±0.03	(25) 0.93±0.04	(0) -	(0) -	(82) 0.92±0.03
g_{440}	Ersa	(993) 0.69±0.02	(538) 0.70±0.03	(158) 0.72±0.05	(518) 0.70±0.03	(2207) 0.69±0.03
	Palma	(809) 0.69±0.03	(548) 0.71±0.03	(177) 0.68±0.04	(184) 0.69±0.03	(1718) 0.70±0.03
ARF_{BOA}	Ersa	(413) -17.5±9.5	(205) -13.6±10.0	(23) -17.6±8.3	(195) -18.0±9.2	(836) -16.7±9.7
$[W \cdot m^{-2}]$	Palma	(282) -22.8±13.4	(193) -16.5±12.1	(14) -6.7±3.3	(65) -9.6±6.0	(554) -18.7±13.2
ARF_{TOA}	Ersa	(413) -12.8±7.0	(205) -9.7±6.6	(23) -7.4±4.9	(195) -10.9±5.7	(836) -11.4±6.7
$[W \cdot m^{-2}]$	Palma	(282) -13.0±6.8	(193) -10.7±6.5	(14) 5.5±2.8	(65) -6.9±3.6	(554) -11.3±6.7
$ARFE_{BOA}$	Ersa	(413) -139.1±23.6	(205) -137.8±18.8	(23) -182.9±31.4	(195) -157.9±39.7	(836) -144.4±29.3
$[W \cdot m^{-2} \cdot AOD_{550}^{-1}]$	Palma	(282) -136.4±40.9	(193) -129.6±27.4	(14) -130.7±13.9	(65) -122.0±24.6	(554) -132.2±34.8
$ARFE_{TOA}$	Ersa	(413) -101.2±10.2	(205) -100.7±12.1	(23) -74.7±11.6	(195) -96.3±15.1	(836) -99.2±12.8
$[W \cdot m^{-2} \cdot AOD_{550}^{-1}]$	Palma	(282) -79.7±18.9	(193) -88.5±15.4	(14) -107.0±13.3	(65) -93.8±12.9	(554) -85.1±18.1

Table 3. Summary of the seasonal variations of the following aerosol properties: SSA_{440}, g_{440}, the solar aerosol radiative forcing (ARF) and the solar aerosol radiative forcing efficiency (ARFE) at Ersa and Palma derived from AERONET level 2.0 inversion products available in the period 2011 – 2015. BOA and TOA stand for bottom of the atmosphere and top of the atmosphere, respectively. The values of SSA_{440} are given for $50 < SZA < 80º$ and $AOD_{440} > 0.40$. The values of ARF and ARFE are given for $50 < SZA < 60º$.

Figure 1. Geographical situation of Ersa, Palma and Alborán AERONET stations in the western Mediterranean Basin. Credits: map adapted from Google Earth.

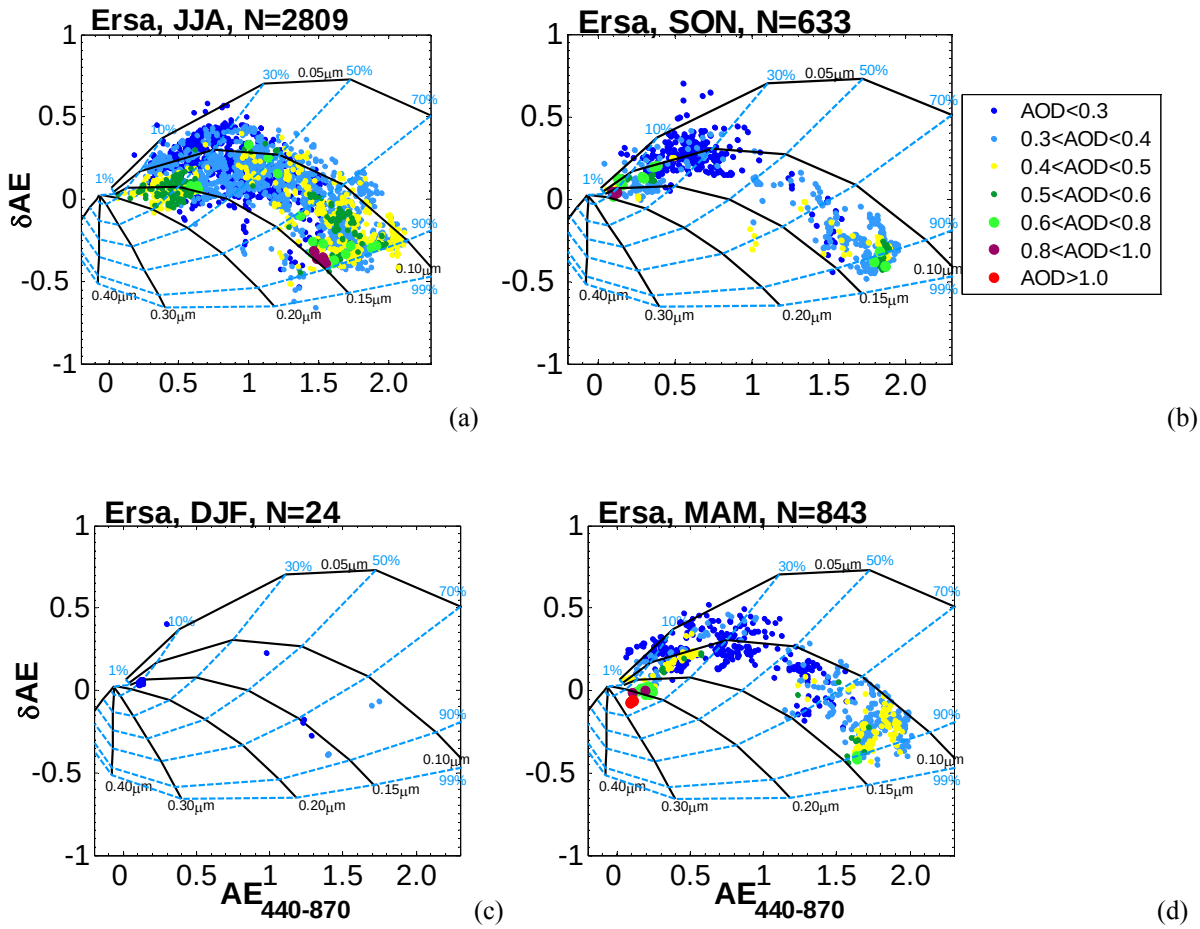

Figure 2. Ångström exponent difference ($\delta AE = AE_{440\text{-}675} - AE_{675\text{-}870}$) as a function of the Ångström exponent calculated between 440 and 870 nm ($AE_{440\text{-}870}$) at Ersa during (a) summer, (b) autumn, (c) winter and (d) spring, for the whole 2011-2015 AERONET level 2.0 AOD dataset. Only points with $AOD_{675} > 0.15$ are represented. However the AOD plotted is AOD_{440} (and not AOD_{675}) in order to be directly comparable with the AERONET inversion criteria based on AOD_{440}. The legend applies for all plots. A bimodal, lognormal size distribution and a refractive index of 1.4-0.001*i* were considered to construct the grid. The black solid lines are each for a fixed fine mode radius and the dashed blue lines for a fixed fraction of the fine mode contribution to the AOD at 675 nm. In this figure and in the rest of the paper N represents the number of points or observations shown in the plot or used to calculate the means shown in the plot.

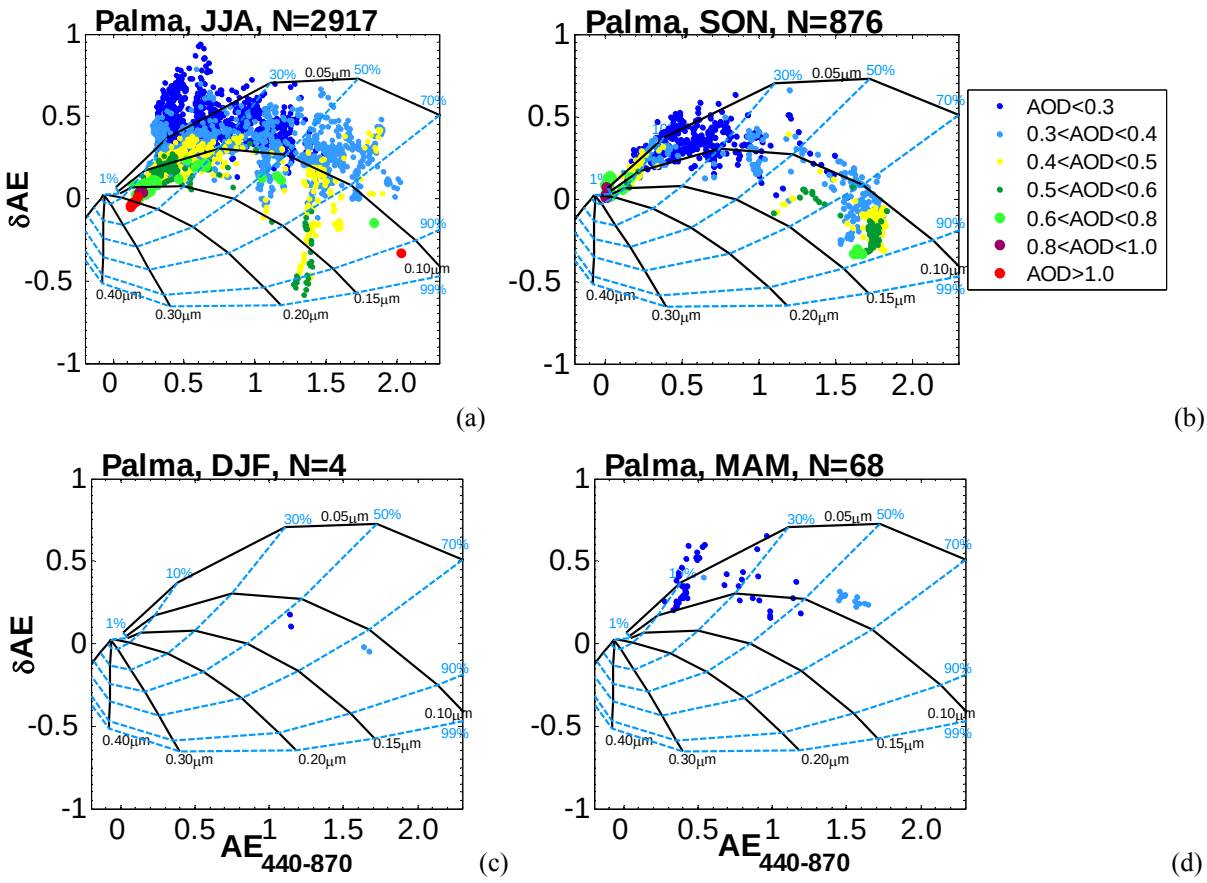

Figure 3. Ångström exponent difference ($\delta AE = AE_{440\text{-}675} - AE_{675\text{-}870}$) as a function of the Ångström exponent calculated between 440 and 870 nm ($AE_{440\text{-}870}$) at Palma during (a) summer, (b) autumn, (c) winter and (d) spring, for the whole 2011-2015 AERONET level 2.0 AOD dataset. Only points with $AOD_{675} > 0.15$ are represented. However the AOD plotted is AOD_{440} (and not AOD_{675}) in order to be directly comparable with the AERONET inversion criteria based on AOD_{440}. The legend applies for all plots. A bimodal, lognormal size distribution and a refractive index of 1.4-0.001*i* were considered to construct the grid. The black solid lines are each for a fixed fine mode radius and the dashed blue lines for a fixed fraction of the fine mode contribution to the AOD at 675 nm.

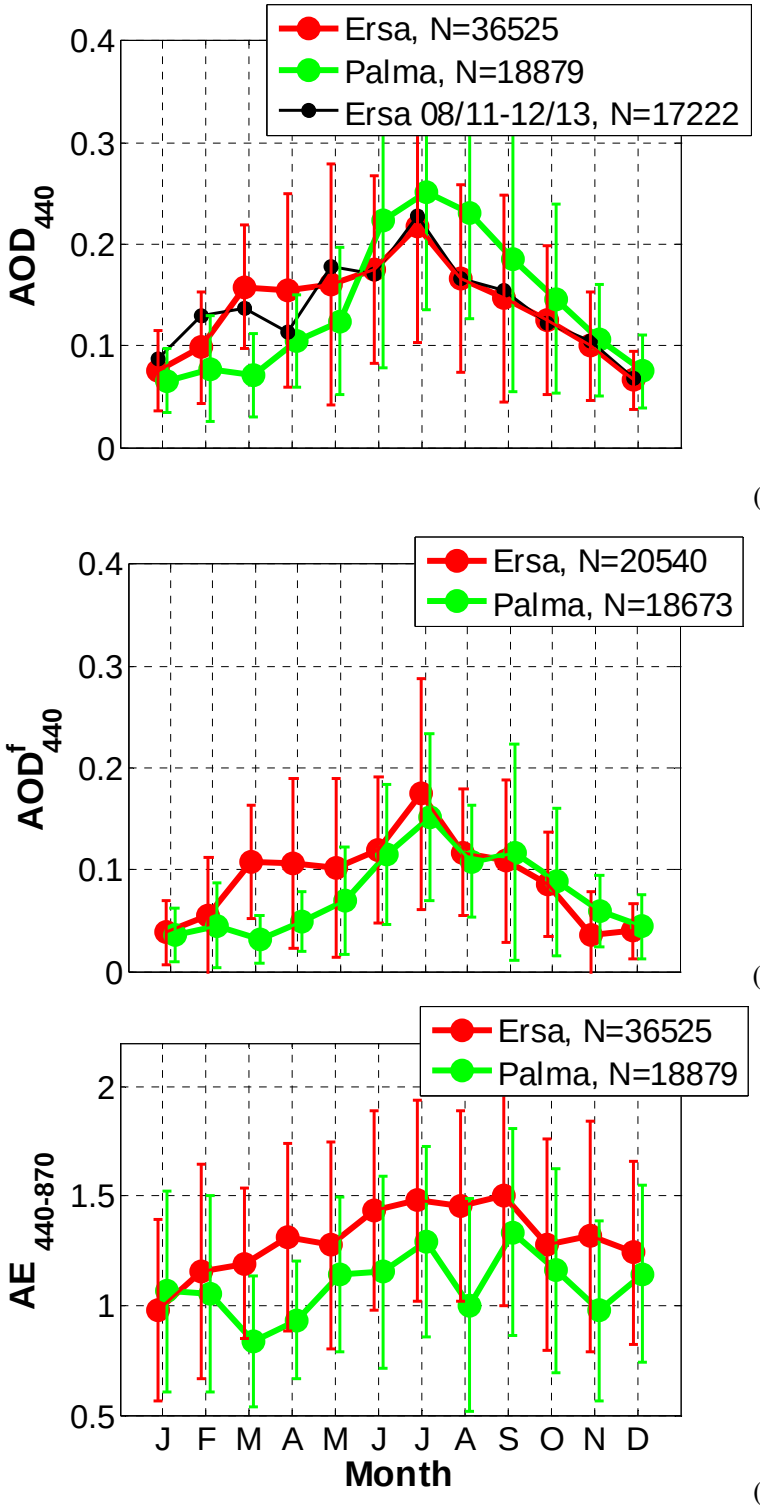

Figure 4. Monthly average variations calculated with instantaneous measurements of a) AOD_{440}; b) AOD^{f}_{440}; and c) $AE_{440–870}$ derived from AERONET level 2.0 inversion products available in the period 2011 – 2015. The error bars represent the standard deviation. On the AOD_{440} plot we have also plotted the monthly values at Ersa calculated over the limited period for which data are also available at Palma, i.e. August 2011 – December 2013.

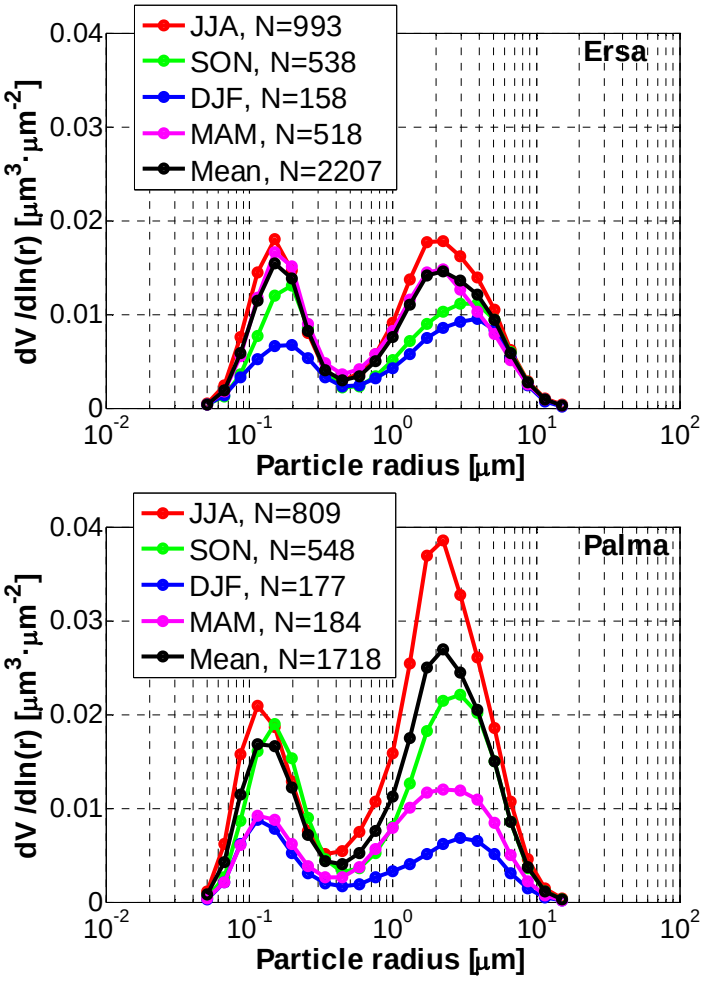

Figure 5. Seasonal variation of the particle volume size distribution at (a) Ersa and (b) Palma derived from AERONET level 2.0 inversion products available in the period 2011 – 2015.

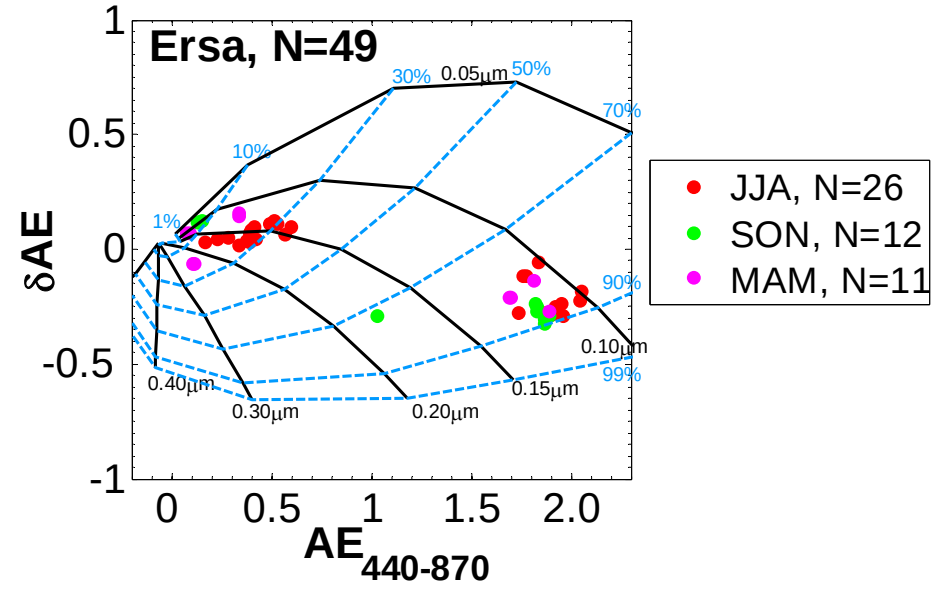

(a)

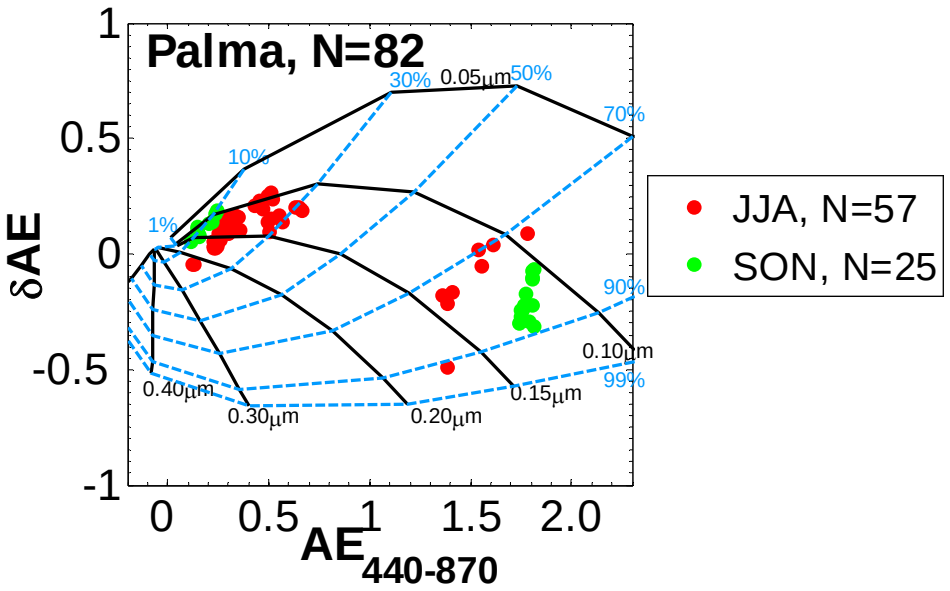

(b)

Figure 6. Ångström exponent difference ($\delta AE = AE_{440\text{-}675} - AE_{675\text{-}870}$) as a function of the Ångström exponent calculated between 440 and 870 nm ($AE_{440\text{-}870}$) at (a) Ersa and (b) Palma, derived from AERONET level 2.0 inversion products available in the period 2011 – 2015, which means that the following criteria apply on these data: $50 < SZA < 80^{\circ}$ and $AOD_{440} > 0.4$. A bimodal, lognormal size distribution and a refractive index of 1.4-0.001*i* were considered to construct the grid. The black solid lines are each for a fixed fine mode radius and the dashed blue lines for a fixed fraction of the fine mode contribution to the AOD at 675 nm.

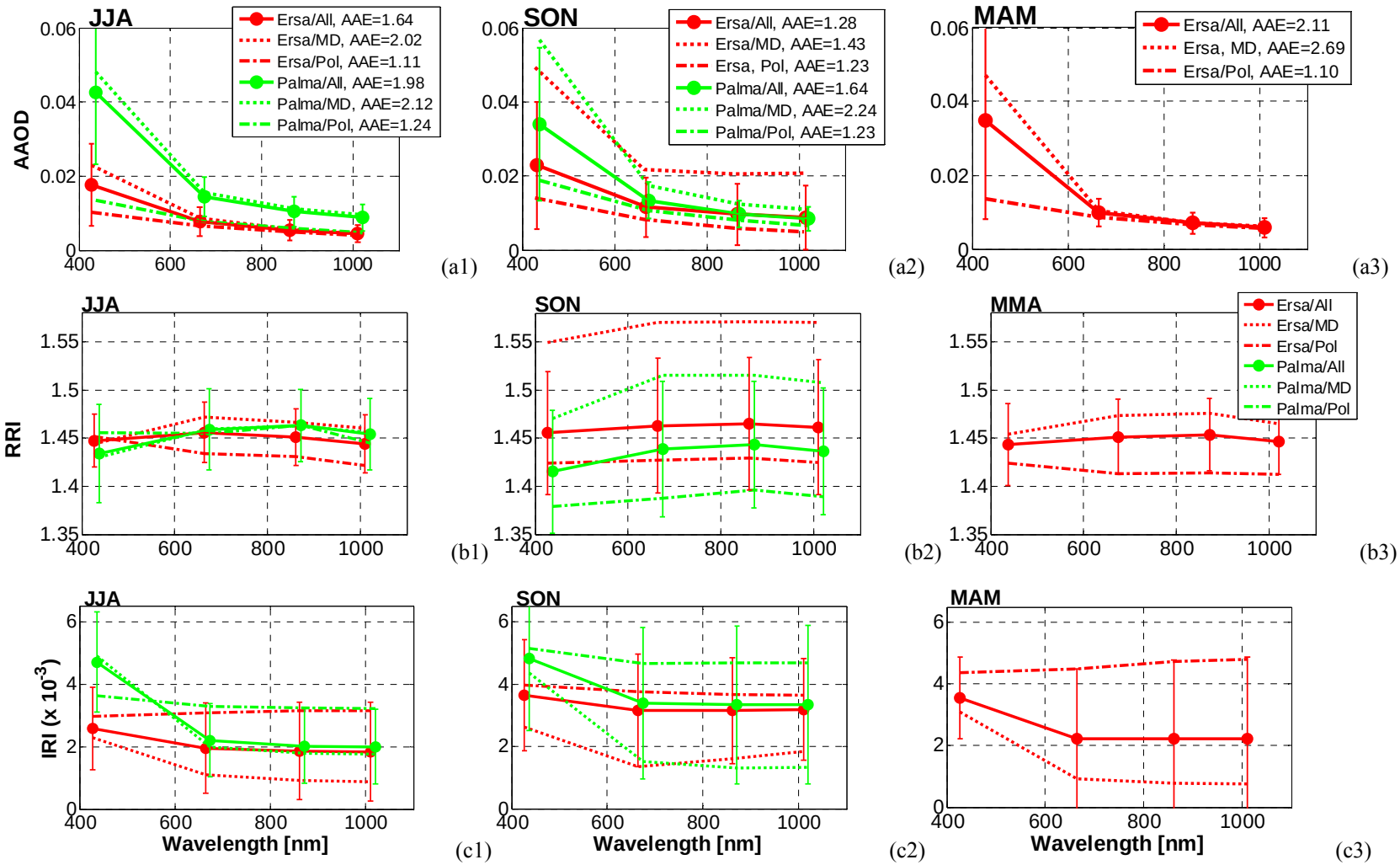

Figure 7. Seasonal variation of the spectra of (a) the aerosol absorption optical depth (AAOD), (b) the real part of the refractive index (RRI) and (c) the imaginary part of the refractive index (IRI) during (1) summer, (2) autumn and (3) spring, derived from AERONET level 2.0 inversion products available in the period 2011-2015. The legend in plot (b3) applies for all plots (b) and (c). All three parameters are retrieved with the following restrictions: $50 < SZA < 80^{o}$ and $AOD_{440} > 0.4$. The error bars represent the standard deviation. The seasonal mean is represented for the whole dataset (All), and separately for mineral dust (MD) and pollution (Pol) cases determined with the classification obtained from Figure 6 (see first paragraph of Section 5.3).

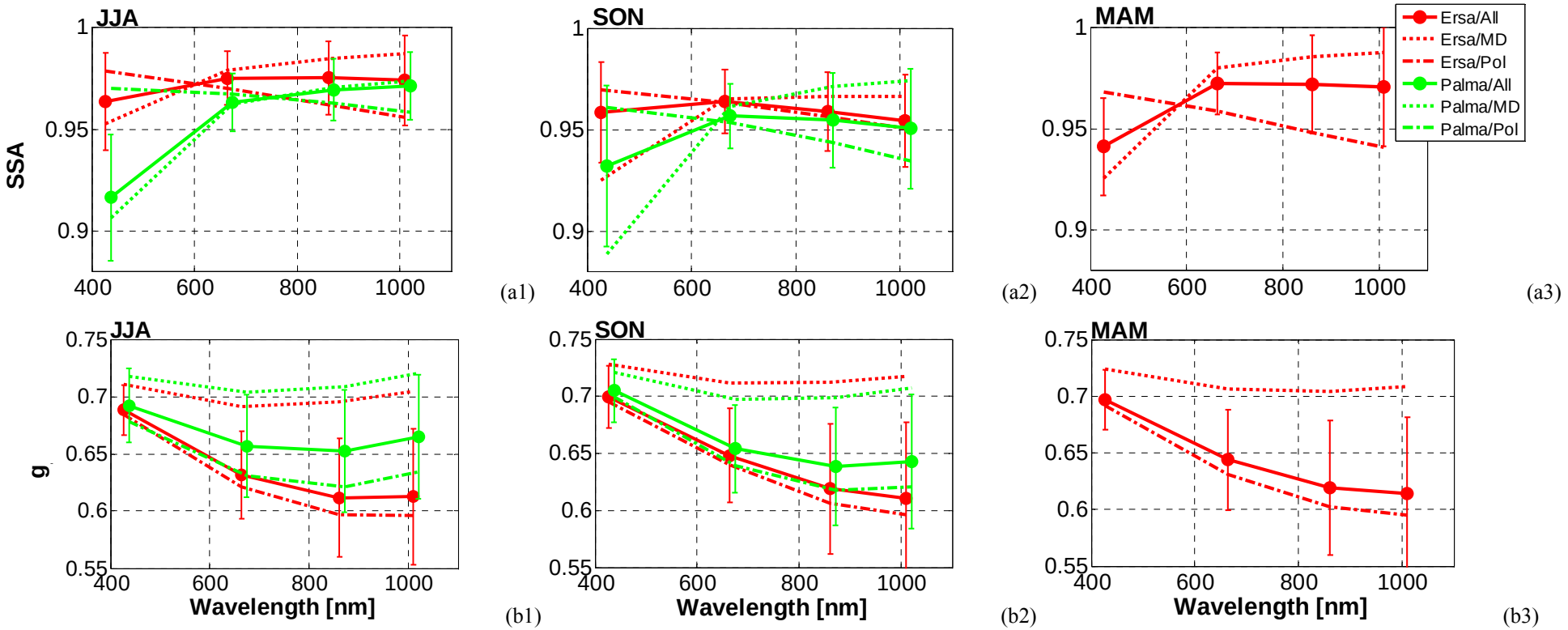

Figure 8. Seasonal variation of the spectra of (a) the single scattering albedo (SSA) and (b) the asymmetry factor (*g*) at 440 nm during (1) summer, (2) autumn and (3) spring, derived from AERONET level 2.0 inversion products available in the period 2011-2015. The legend in plot (a3) applies for all plots (a) and (b). SSA is retrieved with the following restrictions: $50 < SZA < 80^{o}$ and $AOD_{440} > 0.4$. The error bars represent the standard deviation. The seasonal mean is represented for the whole dataset (All), and separately for mineral dust (MD) and pollution (Pol) cases determined with the classification obtained from Figure 6 (see first paragraph of Section 5.3).

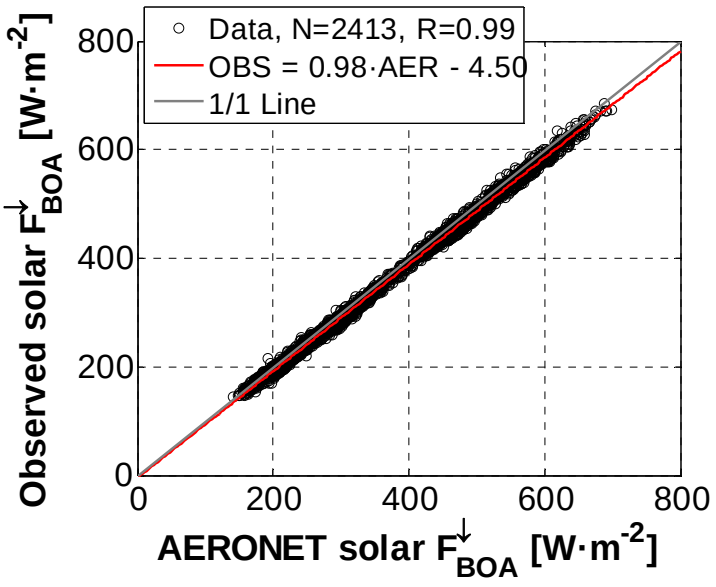

(a)

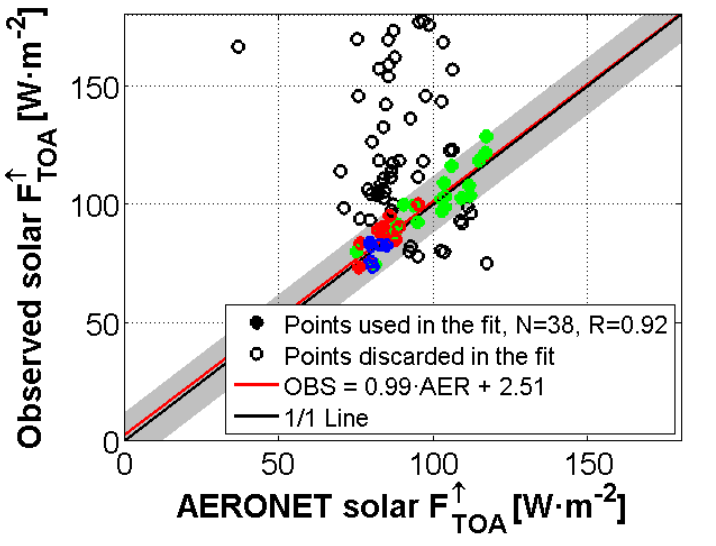

(b)

Figure 9. (a) Observed SolRad-Net level 1.5 versus modeled AERONET level 2.0 instantaneous solar downward fluxes at the surface in Barcelona over the period May 2009 – October 2014; (b) Observed CERES versus modeled AERONET level 1.5 instantaneous solar upward fluxes at the TOA at Ersa (2008 – 2014, red solid bullets), Palma (2011 – 2014, green solid bullets) and Alborán (2011 – 2012, blue solid bullets). The maximum time difference allowed between observed and AERONET fluxes is ± 1 and ± 15 min. at the BOA and TOA, respectively. In (b) the shaded area indicates the CERES uncertainty, namely ± 13.5 W·m^{-2} around the 1/1 line; and the open bullets represent the pairs of points (CERES, AERONET), shown for completeness but discarded in the fit, that have a difference larger than CERES uncertainty.

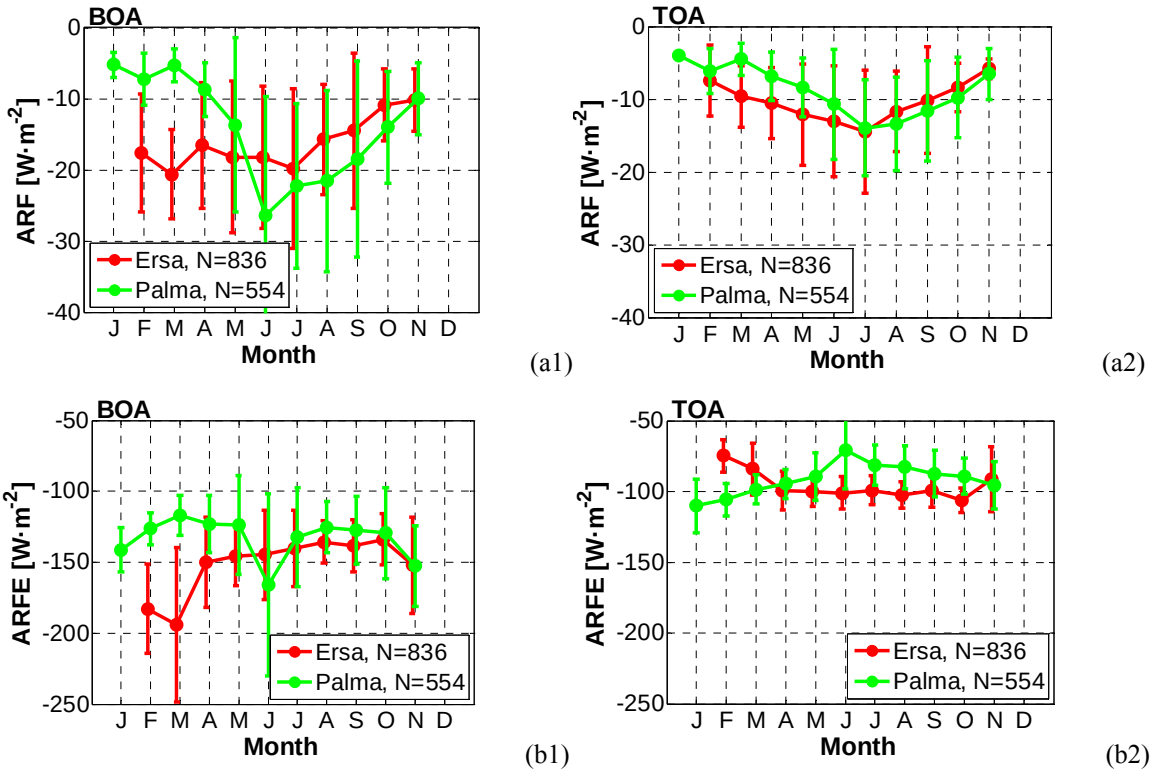

Figure 10. Monthly variation of (a) the solar aerosol radiative forcing (ARF) and of (b) the solar aerosol radiative forcing efficiency (ARFE) at the (1) BOA and (2) TOA, derived from AERONET level 2.0 inversion products available in the period 2011-2015. Both the ARF and the ARFE were estimated for $50 \leq SZA \leq 60^{o}$. The error bars represent the standard deviation.

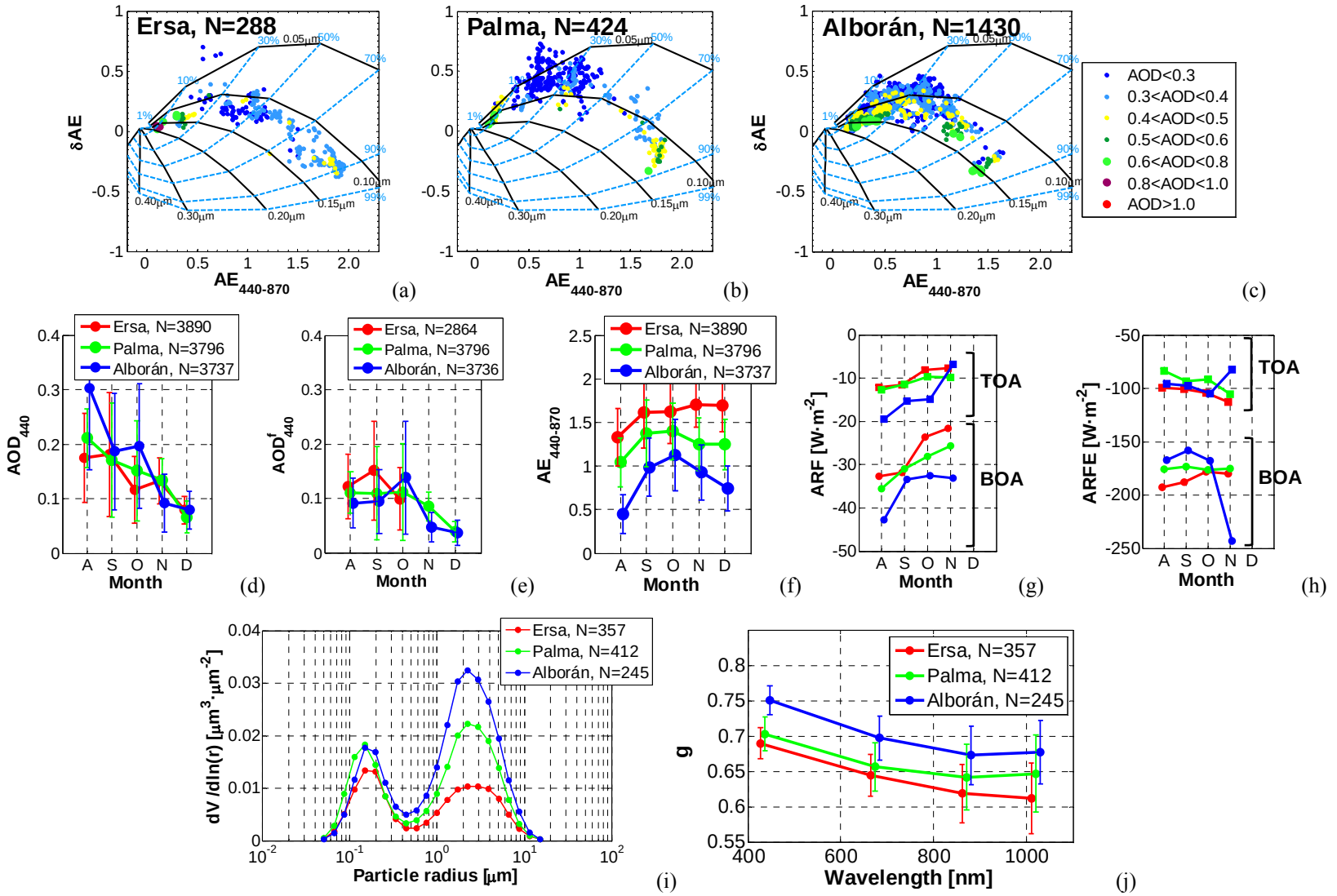

Figure 11. (δAE, AE) plot at (a) Ersa, (b) Palma and (c) Alborán over the whole period; monthly variations of (d) AOD_{440}, (e) AOD^{f}_{440}, (f) $AE_{440\text{-}870}$, (g) ARF and (h) ARFE; (i) size distribution and (j) spectra of *g* averaged over the whole period. The data are from AERONET level 2.0 inversion products during the period August to December 2011. The numbers of points in the plots (g) and (h) (not indicated in the plots for the sake of clarity) are 123, 133 and 101 for Ersa, Palma and Alborán, respectively. The color code is the same in all figures (d)-(j): red, green and blue for Ersa, Palma and Alborán, respectively. In (g)-(h) the error bars have been omitted for the sake of clarity.